

# Stability Analysis of the Instantaneous Bethe-Salpeter Equation and the Consequences for Meson Spectroscopy

J. Parramore

*Department of Physics and Supercomputer Computations Research Institute,  
Florida State University, Tallahassee, FL 32306*

H.-C. Jean

*Department of Physics and Supercomputer Computations Research Institute,  
Florida State University, Tallahassee, FL 32306*

J. Piekarewicz

*Supercomputer Computations Research Institute,  
Florida State University, Tallahassee, FL 32306*

(August 8, 2018)

## Abstract

We investigate the light and heavy meson spectra in the context of the instantaneous approximation to the Bethe-Salpeter equation (Salpeter's equation). We use a static kernel consisting of a one-gluon-exchange component and a confining contribution. Salpeter's equation is known to be formally equivalent to a random-phase-approximation equation; as such, it can develop imaginary eigenvalues. Thus, our study can not be complete without first discussing the stability of Salpeter's equation. The stability analysis limits the form of the kernel and reveals that, contrary to the usual assumption, the confining component can not transform as a Lorentz scalar; it must transform as the timelike component of a vector. Moreover, the stability analysis sets an upper limit on the size of the one-gluon-exchange component; the value for the critical coupling is determined through a solution of the "semirelativistic" Coulomb problem. These limits place important constraints on the interaction and suggest that a more sophisticated model is needed to describe the light and heavy quarkonia.

PACS number(s): 11.10.St,12.40.Qq,14.40.-n

## I. INTRODUCTION

In hadron-structure theory one is interested in describing the hadron as a relativistic composite system. To date, most basic properties of hadrons cannot yet be derived from QCD—the fundamental theory of the strong interactions. Note, however, that QCD sum rules can place some constraints regarding quark-distribution amplitudes in mesons and baryons [1,2]. With the advent of more powerful computing facilities, lattice gauge theory [3] should provide an increasingly useful means of studying hadronic physics. Yet, at the present time it does not provide a convenient framework for a systematic study of a large variety of hadronic phenomena. Specifically, with the commission of state-of-the-art facilities, such as CEBAF<sup>1</sup>, other nonperturbative techniques will be required which can be used to incorporate phenomena at many different length scales within a single theoretical framework.

To a large extent our current understanding of hadronic structure is based on the non-relativistic constituent quark model [4,5]. Meson properties are well reproduced by a phenomenological potential consisting of the sum of a short-range one-gluon exchange (OGE) component and a long-range confining contribution. A quantitative description of meson masses, their static properties and decay rates count among the many successes of the model. Generally, one would prefer to have a relativistic and manifestly covariant model. For example, a covariant formalism will enable one to relate the wave function (or vertex function) in different frames. This becomes essential for calculating hadronic form factors at finite momentum transfer.

The starting point for most relativistic studies of the meson spectrum is the covariant Bethe-Salpeter equation [6]. The Bethe-Salpeter equation can be regarded as the relativistic generalization of the Lippmann-Schwinger equation. However, the Bethe-Salpeter equation, being covariant, depends on the zeroth component of the relative four-momentum (i.e., the relative energy). Aside from the technical difficulties encountered in handling this extra degree of freedom, one must decide in the present case how to generalize the essentially nonrelativistic quark-antiquark potential to four dimensions—a nontrivial task to carry out correctly. The difficulty in dealing with the relative energy has led to many different approximations to the Bethe-Salpeter equation wherein one works within a three-dimensional reduction but attempts to retain fundamental physical principles. There is no obviously correct method. Thus, one should study different three-dimensional reductions in the hope of isolating model-independent results. Here we work within the instantaneous Bethe-Salpeter framework (Salpeter's framework). Although retardation effects and manifest covariance are lost, one retains relativistic kinematics, the relativistic character of the potential, and the Dirac structure of positive- and negative-energy states.

The use of the instantaneous approximation commonly employed in the literature entails other problems besides the loss of retardation and manifest covariance; Salpeter's bound-state equation is represented by a *nonhermitian* Hamiltonian. Indeed, it has been recognized [7–10] that Salpeter's equation is identical in structure to a random-phase-approximation (RPA) equation familiar from the study of nuclear collective excitations [11]. Thus, it can be rewritten as a hermitian eigenvalue equation—but for the square of the

---

<sup>1</sup>The Continuous Electron Beam Accelerator Facility

energy. This suggests the possibility of imaginary eigenvalues which would signal the onset of an instability. For our problem of interest these imaginary solutions are unphysical and their appearance can be precluded by limiting the form of the kernel. This is achieved through a stability analysis of Salpeter's equation. We should stress that any study based on Salpeter's equation is not complete until the stability analysis is performed. The main goal of this paper is to present the stability analysis and to examine the implications for the meson spectra.

We have organized the paper as follows. In Sec. II, Salpeter's equation is presented and the method used to solve it is reviewed. In Section III, we study the interaction kernel for the particular Lorentz structures of interest. The stability analysis for the confining part of the kernel is reviewed [9] and the analysis for the OGE component developed. As a result of the stability analysis the form of the instantaneous kernel is constrained. We examine the consequences of these constraints on the heavy- and light-meson spectroscopy in Section IV. Finally, our concluding remarks are presented in Section V.

## II. FORMALISM

### A. Salpeter's Equation

In the Salpeter formalism [12], the bound-state spectrum is generated as a solution to the instantaneous Bethe-Salpeter equation in the ladder approximation. In this approximation, the irreducible Bethe-Salpeter kernel is given by

$$V(x_1, x_2) \equiv V(\mathbf{x}_1, \mathbf{x}_2) . \quad (1)$$

In Ref. [9], the derivation of Salpeter's equation was illustrated using Green's function methods, which yielded the following eigenvalue equation for the Salpeter wave function  $\chi^E$ :

$$\chi_{\alpha\sigma}^E(\mathbf{x}_1, \mathbf{y}_2) = \int d^3z_1 d^3z_2 G_{\alpha\eta';\xi\sigma}^{(0)}(\mathbf{x}_1, \mathbf{z}_2; \mathbf{z}_1, \mathbf{y}_2; E) V_{\xi\eta;\xi'\eta'}(\mathbf{z}_1, \mathbf{z}_2) \chi_{\xi'\eta}^E(\mathbf{z}_1, \mathbf{z}_2) , \quad (2)$$

where the Salpeter wave function is defined by

$$\chi_{\alpha\sigma}^E(\mathbf{x}_1, \mathbf{y}_2) \equiv \langle \Psi_0 | \psi_\alpha(\mathbf{x}_1) \bar{\psi}_\sigma(\mathbf{y}_2) | \Psi_E \rangle , \quad (3)$$

$G^{(0)}$  is the free two-body propagator in the instantaneous approximation (IA),  $\Psi_0$  represents the vacuum, and  $\Psi_E$  represents the bound state with energy  $E$ . Expanding the fermion fields in a single-particle basis and using the properties of the free two-body Green's function then gives

$$\chi_{\alpha\sigma}^E(\mathbf{x}_1, \mathbf{y}_2) = \sum_{\mathbf{k}_1 s_1; \mathbf{k}_2 s_2} \left( \left[ U_{\mathbf{k}_1 s_1}(\mathbf{x}_1) \right]_\alpha \left[ \bar{V}_{\mathbf{k}_2 s_2}(\mathbf{y}_2) \right]_\sigma B_{s_1 s_2}(\mathbf{k}_1, \mathbf{k}_2) + \left[ V_{\mathbf{k}_1 s_1}(\mathbf{x}_1) \right]_\alpha \left[ \bar{U}_{\mathbf{k}_2 s_2}(\mathbf{y}_2) \right]_\sigma D_{s_1 s_2}(\mathbf{k}_1, \mathbf{k}_2) \right) , \quad (4)$$

where the Salpeter amplitudes  $B$  and  $D$  are defined by

$$B_{s_1 s_2}(\mathbf{k}_1, \mathbf{k}_2) \equiv \langle \Psi_0 | b_{s_1}(\mathbf{k}_1) d_{s_2}(\mathbf{k}_2) | \Psi_E \rangle , \quad (5)$$

$$D_{s_1 s_2}(\mathbf{k}_1, \mathbf{k}_2) \equiv \langle \Psi_0 | d_{s_1}^\dagger(\mathbf{k}_1) b_{s_2}^\dagger(\mathbf{k}_2) | \Psi_E \rangle , \quad (6)$$

and contain all dynamical information about the bound state.

Salpeter's equations are more conveniently expressed in an angular momentum basis. Projecting out the Salpeter amplitudes, expressing Salpeter's equations for  $B$  and  $D$  in the center of momentum frame, and introducing the partial-wave decomposition of the amplitudes in terms of total  $L$  and  $S$  coupled to the total angular momentum  $J$  of the bound state

$$B_{s_1 s_2}(\mathbf{k}) = \sum_{SM_S LM_L JM} \left\langle \frac{1}{2} s_1; \frac{1}{2} s_2 | SM_S \right\rangle \langle LM_L; SM_S | JM \rangle Y_{L, M_L}(\hat{k}) B_{LSJM}(k) , \quad (7)$$

$$(-)^{1-s_1-s_2} D_{-s_1-s_2}(\mathbf{k}) = \sum_{SM_S LM_L JM} \left\langle \frac{1}{2} s_1; \frac{1}{2} s_2 | SM_S \right\rangle \langle LM_L; SM_S | JM \rangle Y_{L, M_L}(\hat{k}) D_{LSJM}(k) , \quad (8)$$

one can write Salpeter's equations in an angular momentum basis as

$$[+E - 2E_k] b_{LSJ}(k) = \int_0^\infty \frac{dk'}{(2\pi)^3} \sum_{L'S'} \left\{ \langle k; LSJ | V^{++} | k'; L'S'J \rangle b_{L'S'J}(k') + \langle k; LSJ | V^{+-} | k'; L'S'J \rangle d_{L'S'J}(k') \right\} , \quad (9)$$

$$[-E - 2E_k] d_{LSJ}(k) = \int_0^\infty \frac{dk'}{(2\pi)^3} \sum_{L'S'} \left\{ \langle k; LSJ | V^{-+} | k'; L'S'J \rangle b_{L'S'J}(k') + \langle k; LSJ | V^{--} | k'; L'S'J \rangle d_{L'S'J}(k') \right\} , \quad (10)$$

with  $b(k) \equiv kB(k)$  and  $d(k) \equiv kD(k)$ . For local interactions, such as the ones considered here, the matrix elements of the potential are given by (a sum over greek indices is implicitly assumed, and  $\bar{\alpha} \equiv 1 - \alpha$ )

$$\begin{aligned} \langle k; LSJ | V^{++} | k'; L'S'J \rangle &= \langle k; LSJ | V^{--} | k'; L'S'J \rangle \\ &= \sum_{\mathcal{L}\mathcal{S}} (-1)^{\alpha+\beta} \mathcal{F}_{\mathcal{L}\mathcal{S}; LSJ}^{\alpha\beta}(k) \langle \mathcal{S} | [V_{\mathcal{L}}(k, k')]_{\alpha\beta; \alpha'\beta'} | \mathcal{S} \rangle \mathcal{F}_{\mathcal{L}\mathcal{S}; L'S'J}^{\alpha'\beta'}(k') , \end{aligned} \quad (11)$$

$$\begin{aligned} \langle k; LSJ | V^{+-} | k'; L'S'J \rangle &= \langle k; LSJ | V^{-+} | k'; L'S'J \rangle \\ &= \sum_{\mathcal{L}\mathcal{S}} (-1)^{\alpha+\beta+\mathcal{L}} \mathcal{F}_{\mathcal{L}\mathcal{S}; LSJ}^{\alpha\beta}(k) \langle \mathcal{S} | [V_{\mathcal{L}}(k, k')]_{\alpha\beta; \alpha'\beta'} | \mathcal{S} \rangle \mathcal{F}_{\mathcal{L}\mathcal{S}; L'S'J}^{\alpha'\beta'}(k') . \end{aligned} \quad (12)$$

where

$$\mathcal{F}_{\mathcal{L}\mathcal{S}; LSJ}^{\alpha\beta}(k) = C_{\alpha\beta}(k) \sum_{\lambda} \langle \alpha 0; \beta 0 | \lambda 0 \rangle \langle \mathcal{L}\mathcal{S} J | [Y_{\lambda}(\sigma_{\alpha}\sigma_{\beta})_{\lambda}]_0 | \mathcal{L}\mathcal{S} J \rangle , \quad (13)$$

$$C_{\alpha\beta}(k) = \sqrt{4\pi} (-1)^{\alpha} \left[ \frac{E_k + M}{2E_k} \right] \xi_{\alpha}(k) \xi_{\beta}(k) ; \quad \xi_{\alpha}(k) = \begin{cases} 1 & \text{if } \alpha = 0 ; \\ \frac{k}{E_k + M} & \text{if } \alpha = 1. \end{cases} \quad (14)$$

and  $E_k \equiv \sqrt{k^2 + M^2}$ , with  $M$  the constituent quark mass. (The equal-mass case is considered here; however, the extension to unequal masses is straightforward.) The quantum numbers  $L, S$  range only over the values allowed by  $J^\pi$ , and correspond to the usual “non-relativistic” quantum numbers, while  $\mathcal{L}, \mathcal{S}$  can take on all values allowed by the coupling to  $J$ , thus reflecting the role of relativity in the calculation. For  $E > 0$ , the amplitudes  $b, d$  satisfy the RPA normalization condition [13]

$$\sum_{LS} \int_0^\infty \frac{dk}{(2\pi)^3} [b_{LSJ}^2(k) - d_{LSJ}^2(k)] = 1. \quad (15)$$

Eqs. (9) and (10) are similar to the equations in Ref. [10] for the two-fermion case. This form is used for convenience, as the two can be related by charge conjugation.

## B. The RPA Equation

Salpeter’s equation can be cast in the following compact matrix form:

$$\begin{pmatrix} H^{++} & H^{+-} \\ -H^{+-} & -H^{++} \end{pmatrix} \begin{pmatrix} B \\ D \end{pmatrix} = E \begin{pmatrix} B \\ D \end{pmatrix}, \quad (16)$$

where the matrix elements of the “Hamiltonian” are given by

$$\langle k; LSJ | H^{++} | k'; L' S' J \rangle = \langle k; LSJ | V^{++} | k'; L' S' J \rangle + 2E_k (2\pi)^3 \delta(k - k') \delta_{LL'} \delta_{SS'}, \quad (17)$$

$$\langle k; LSJ | H^{+-} | k'; L' S' J \rangle = \langle k; LSJ | V^{+-} | k'; L' S' J \rangle. \quad (18)$$

One recognizes that Salpeter’s eigenvalue equation, as given by Eq. (16), has the same algebraic structure as an RPA equation [7–10]. Having identified the algebraic (RPA) structure of Salpeter’s equation, the same formalism developed by Thouless in his study of nuclear collective excitations [11] will be employed. Salpeter’s, and in general any RPA-like, equation can be rewritten as a Hermitian eigenvalue equation for the square of the energy [13,14]. This implies that while the square of the energy is guaranteed to be real, the energy itself might not. The appearance of solutions having  $E^2 < 0$  signals, in the context of nuclear collective excitations, an instability of the ground state against the formation of particle-hole pairs — a collective mode with imaginary energy can build up indefinitely. Thouless has shown that the stability of the nuclear ground state depends on the Hermitian matrix

$$\begin{pmatrix} H^{++} & H^{+-} \\ H^{+-} & H^{++} \end{pmatrix} \quad (19)$$

being positive-definite—all its eigenvalues must be greater than zero [11,13,14]. This condition is equivalent to requiring that both the sum and difference matrices

$$H^+ \equiv (H^{++} + H^{+-}), \quad (20)$$

$$H^- \equiv (H^{++} - H^{+-}), \quad (21)$$

be positive-definite [14]. In this form, the stability condition of Salpeter’s equation is reduced to finding the eigenvalues of the two Hermitian matrices  $H^+$  and  $H^-$ . Thus, the existence of

a single negative eigenvalue, of either  $H^+$  or  $H^-$ , suffices to signal the instability. It is this criterion that was employed in Ref. [9] to examine the Lorentz structure of the confining potential; also, it will be used in this work to set limits on the strong coupling for the instantaneous OGE kernel in Salpeter's equation. With these limits in hand, one is then able to carry out (see Section IV) a study of the meson spectra in the framework of Salpeter's equation.

### C. Numerical Solution of Salpeter's Equation

Salpeter's equation is solved via expansion of the Salpeter amplitudes in a suitable basis, thus enabling one to treat the instantaneous confining and Coulomb kernels in configuration representation and the relativistic kinetic energy operator in momentum representation, where they are respectively local. Here and in Ref. [9], one uses the radial eigenfunctions of the nonrelativistic harmonic oscillator,  $R_{nL}$ , to expand the two amplitudes  $B_{LSJ}$  and  $D_{LSJ}$  in terms of unknown coefficients

$$B_{LSJ}(k) = \sum_n^{n_{max}} B_{nLSJ} R_{nL}(k) \quad (22)$$

$$D_{LSJ}(k) = \sum_n^{n_{max}} D_{nLSJ} R_{nL}(k) \quad , \quad (23)$$

up to  $n=0, \dots, n_{max}$  nodes in the basis, for a finite basis. (Since the interaction is spherically symmetric, the magnetic quantum number  $M$  only denotes a  $2J + 1$ -degeneracy and plays no dynamical role; hence it can be dropped.) This procedure results in a matrix equation for the unknown coefficients  $B_{nLSJ}$  and  $D_{nLSJ}$  which can be diagonalized using the method developed by Ullah and Rowe [13]. Upon diagonalization, one obtains  $E^2$  and the (previously) unknown coefficients from which one then can reconstruct the two amplitudes  $B_{LSJ}$  and  $D_{LSJ}$ , and, ultimately, the Salpeter wave function  $\chi^E$ .

### III. STABILITY ANALYSIS OF SALPETER'S EQUATION

The stability analysis is performed by using potentials  $V(r)$  having scalar, timelike-vector, and vector Lorentz structures

$$V(r)\Gamma_1\Gamma_2 = V(r) \begin{cases} \mathbf{1}_1\mathbf{1}_2, & \text{for scalar,} \\ \gamma_1^0\gamma_2^0, & \text{for timelike,} \\ \gamma_1^\mu\gamma_{2\mu}, & \text{for vector,} \end{cases} \quad (24)$$

which are the relevant structures for the meson problem. The analysis is concentrated on the pseudoscalar ( $J^\pi=0^-$ ) channel; with  $L=S=0$ , this is the first channel where the instability is likely to develop. For this case, Salpeter's equation, for the reduced amplitudes  $b(k) \equiv kB(k)$  and  $d(k) \equiv kD(k)$ , takes the following form

$$(+E - 2E_k) b(k) = \int_0^\infty \frac{dk'}{(2\pi)^3} \left\{ \langle k|V^{++}|k' \rangle b(k') + \langle k|V^{+-}|k' \rangle d(k') \right\} \quad , \quad (25)$$

$$(-E - 2E_k) d(k) = \int_0^\infty \frac{dk'}{(2\pi)^3} \left\{ \langle k|V^{+-}|k' \rangle b(k') + \langle k|V^{++}|k' \rangle d(k') \right\} \quad . \quad (26)$$

In spite of the simplicity of the angular momentum content of this channel, the matrix elements of the potential are complicated by relativistic corrections. We define the angular-momentum components of the potential by

$$V_{\mathcal{L}}(k, k') = (4\pi)^2 \int_0^\infty dr \hat{j}_{\mathcal{L}}(kr) V(r) \hat{j}_{\mathcal{L}}(k'r), \quad (27)$$

with  $\hat{j}_{\mathcal{L}}(x) \equiv x j_{\mathcal{L}}(x)$  being the Ricatti-Bessel function. For scalar and timelike potentials, one has

$$\begin{aligned} & \langle k | V^{++} | k' \rangle \\ &= \left( \frac{E_k + M}{2E_k} \right) \left( \frac{E_{k'} + M}{2E_{k'}} \right) \left\{ [1 + \zeta_k^2 \zeta_{k'}^2] V_0(k, k') \mp 2\zeta_k \zeta_{k'} V_1(k, k') \right\}, \end{aligned} \quad (28)$$

$$\begin{aligned} & \langle k | V^{+-} | k' \rangle \\ &= \left( \frac{E_k + M}{2E_k} \right) \left( \frac{E_{k'} + M}{2E_{k'}} \right) \left\{ [\zeta_k^2 + \zeta_{k'}^2] V_0(k, k') \pm 2\zeta_k \zeta_{k'} V_1(k, k') \right\}, \end{aligned} \quad (29)$$

where the upper (lower) sign in the above expressions should be used for scalar (timelike) potentials. For vector potentials, one has

$$\begin{aligned} & \langle k | V^{++} | k' \rangle \\ &= \left( \frac{E_k + M}{2E_k} \right) \left( \frac{E_{k'} + M}{2E_{k'}} \right) \left\{ [1 + \zeta_k^2 \zeta_{k'}^2] + 3[\zeta_k^2 + \zeta_{k'}^2] \right\} V_0(k, k'), \end{aligned} \quad (30)$$

$$\begin{aligned} & \langle k | V^{+-} | k' \rangle \\ &= \left( \frac{E_k + M}{2E_k} \right) \left( \frac{E_{k'} + M}{2E_{k'}} \right) \left\{ [\zeta_k^2 + \zeta_{k'}^2] + 3[1 + \zeta_k^2 \zeta_{k'}^2] \right\} V_0(k, k'), \end{aligned} \quad (31)$$

where the kinematical variable

$$\zeta_k \equiv \frac{k}{E_k + M} \sim \mathcal{O}\left(\frac{k}{M}\right), \quad (32)$$

has been introduced to quantify the importance of relativity. In particular, for scalar and timelike potentials, relativistic corrections arising from the mixing of positive and negative energy states (as characterized by  $\langle k | V^{+-} | k' \rangle$ ) appear as  $\mathcal{O}\left(\frac{k^2}{M^2}\right)$  relative to the unmixed (Breit) case. This contrasts with the behavior for vector potentials, where both matrix elements contain  $\mathcal{O}(1)$  terms, implying that the contribution of negative-energy states for vector potentials will impact results more than the scalar and timelike cases. This can be seen by taking the nonrelativistic limit ( $\zeta_k, \zeta_{k'} \rightarrow 0$ ):

$$\langle k | V^{++} | k' \rangle \rightarrow \begin{cases} V_0(k, k'), & \text{for scalar and timelike,} \\ V_0(k, k'), & \text{for vector,} \end{cases} \quad (33)$$

$$\langle k | V^{+-} | k' \rangle \rightarrow \begin{cases} 0, & \text{for scalar and timelike,} \\ 3V_0(k, k'), & \text{for vector.} \end{cases} \quad (34)$$

The  $\mathcal{O}(1)$  term in  $V^{+-}$  in the vector case stems from the additional spacelike ( $\gamma_1 \cdot \gamma_2$ ) contribution relative to the scalar and timelike cases, contrary to the usual assumption that  $\gamma_1 \cdot \gamma_2$  induces  $\mathcal{O}\left(\frac{k^2}{M^2}\right)$  corrections to the nonrelativistic potential. One should also note that the  $\gamma_1 \cdot \gamma_2$  contribution mixes upper and lower components via a spin-spin term, thus giving rise to much stronger splittings than either the scalar or timelike cases.

### A. Stability Analysis for the Confining Kernel

In this subsection, the stability analysis carried out in Ref. [9] is reviewed for completeness. For confining potentials, the Fourier transform [Eq. (27)] is ill-defined. Hence, in examining confinement in momentum space in Ref. [9], the following regularization for the spatial part of the potential was employed [15,16]:

$$V(r) = \sigma r e^{-\eta r} \equiv \sigma \frac{\partial^2}{\partial \eta^2} \frac{e^{-\eta r}}{r}. \quad (35)$$

The Fourier transform of the potential is now well behaved and is given by

$$V(\mathbf{k} - \mathbf{k}') = \frac{\partial^2}{\partial \eta^2} \left[ \frac{4\pi\sigma}{(\mathbf{k} - \mathbf{k}')^2 + \eta^2} \right]. \quad (36)$$

Evidently, one is interested in studying the stability of Salpeter's equation in the limit of  $\eta \rightarrow 0$ . The stability analysis required the explicit evaluation of  $V^+$  and  $V^-$ . These were computed with the help of Eqs. (28) and (29)

$$V^+(k, k') \equiv \langle k | V^{++} + V^{+-} | k' \rangle = V_0(k, k'), \quad (37)$$

$$V^-(k, k') \equiv \langle k | V^{++} - V^{+-} | k' \rangle = V_0(k, k') \xi(k, k'), \quad (38)$$

where one introduced relativistic ‘‘correction’’ factors, separately, for scalar and timelike confinement

$$\xi_s(k, k') \equiv \left[ \frac{M^2}{E_k E_{k'}} - \frac{k k'}{E_k E_{k'}} \frac{V_1(k, k')}{V_0(k, k')} \right], \quad (39)$$

$$\xi_v(k, k') \equiv \left[ \frac{M^2}{E_k E_{k'}} + \frac{k k'}{E_k E_{k'}} \frac{V_1(k, k')}{V_0(k, k')} \right]. \quad (40)$$

For both scalar and timelike confining kernels,  $H^+$  remained positive-definite, while  $H^-$  was positive-definite only for timelike confinement, and not for scalar confinement; a scalar confining kernel in Salpeter's equation leads to imaginary-energy solutions—irrespective of the constituent quark mass [9]. Also, if a mixture of scalar and timelike structure for the Lorentz structure of the potential is employed

$$\Gamma \equiv x \gamma_1^0 \gamma_2^0 + (1 - x) \mathbf{1}_1 \mathbf{1}_2, \quad (41)$$

where  $x$  denotes the fraction of timelike structure, then

$$V^+(k, k') = V_0(k, k'), \quad (42)$$

$$V^-(k, k') = V_0(k, k') \left[ \frac{M^2}{E_k E_{k'}} + (2x - 1) \frac{k k'}{E_k E_{k'}} \frac{V_1(k, k')}{V_0(k, k')} \right]. \quad (43)$$

Again,  $H^+$  remains positive definite, while in contrast,  $H^-$  is positive definite only for  $x \geq 1/2$ . Hence, any mix of scalar and timelike Lorentz structures has stable solutions only for  $x$  in the interval  $0.5 \leq x \leq 1$ . This fact will become important in the study of the meson spectra.



## B. Stability Analysis for the Instantaneous OGE Kernel

One now considers the (short-range) OGE part of the kernel. The stability analysis is performed for a pure Coulomb potential, for both timelike and vector Lorentz structures. (Although an OGE kernel of vector Lorentz character will be employed for the spectra analysis, the timelike results are presented here for comparison.) The spatial part of the (instantaneous) Salpeter kernel is

$$V_{OGE}(r) = \frac{-\alpha_s}{r} \quad (44)$$

with the Fourier transform of  $V_{OGE}(r)$  given by

$$V_{OGE}(|\mathbf{k} - \mathbf{k}'|) = \lim_{\eta \rightarrow 0} \left[ \frac{-4\pi\alpha_s}{(\mathbf{k} - \mathbf{k}')^2 + \eta^2} \right]. \quad (45)$$

where  $\alpha_s$  is the strong coupling (taken here to be independent of the quark-antiquark separation  $r$ , or equivalently, of the momentum transfer  $Q$ ).

For the timelike case, one has essentially carried out all necessary manipulations in Ref. [9]. Eqs. (37) and (38) are completely general for any potential with timelike structure, and one only has to calculate the necessary multipoles of the potential in momentum space to complete the analysis. One looks to the  $k = k'$  limit for which the Coulomb singularity structure is manifest. For  $V_0$  and  $V_1$ , one finds (in the  $\eta \rightarrow 0$  limit):<sup>2</sup>

$$V_0(k, k' = k) = -8\pi^2\alpha_s \frac{1}{2} \ln \left( \frac{4k^2}{\eta^2} \right) + \mathcal{O}\left(\frac{\eta^2}{k^2}\right), \quad (46)$$

$$V_1(k, k' = k) = -8\pi^2\alpha_s \frac{1}{2} \left[ \ln \left( \frac{4k^2}{\eta^2} \right) - 1 + \mathcal{O}\left(\frac{\eta^2}{k^2}\right) \right]. \quad (47)$$

with the leading singularities cancelling in forming the ratio

$$\lim_{\eta \rightarrow 0} \frac{V_1(k, k' = k)}{V_0(k, k' = k)} = \lim_{\eta \rightarrow 0} \left[ 1 - \frac{1}{\ln \left( \frac{\eta^2}{4k^2} \right)} + \mathcal{O}(\eta^2/k^2) \right] = 1. \quad (48)$$

and one sees that  $\xi_v(k, k) \rightarrow 1$  again. However, in contrast to the confining potential, the stability of the RPA matrix in present case is not assured, as the “nonrelativistic” equation for  $H^+$  can become unbounded from below for sufficiently large  $\alpha_s$ . This implies the existence of an upper limit on the effective strong coupling that one can use for a timelike Coulomb potential in Salpeter’s equation, which affects the determination of wave functions and spectra within the model. Thus, it becomes necessary to determine an upper limit on  $\alpha_s$  in order to avoid the instability. Before doing this, the vector case will be considered to see if the same problem exists. The matrix elements of the potential are somewhat complex; however,  $V^-$  and  $V^+$  are quite simple:

---

<sup>2</sup>The OGE subscript will be discarded, and future references to  $V$  will be taken as indicating the Coulomb potential, unless otherwise noted.

$$V^+ = 4V_0(k, k'), \quad (49)$$

$$V^- = -2 \left[ \frac{M^2}{E_k E_{k'}} \right] V_0(k, k'). \quad (50)$$

Since the minus sign in  $V_0$  leaves  $V^-$  positive, one sees that  $H^-$  is actually positive-definite, so is bounded from below, and one can concentrate on  $H^+$ .<sup>3</sup> The eigenvalue equation for  $H^+$  is again the “nonrelativistic” Schrödinger problem, but with a strong coupling four times the original  $\alpha_s$ :

$$\alpha \equiv 4\alpha_s.$$

This is a reflection of the strong upper-to-lower coupling induced by the spacelike component of the vector Lorentz structure. Hence, for both timelike and vector cases, one has to determine an upper limit for  $\alpha_s$  at which Salpeter’s equation becomes unbounded, noting that the upper limit for the vector case will be one-fourth that in the timelike case.

### C. Determination of the Ground State Energy at the “Critical Coupling”

Evidently, one is interested in the spectrum of the “semirelativistic” Coulomb Hamiltonian

$$H = 2\sqrt{k^2 + M^2} - \frac{\alpha}{r}; \quad \alpha > 0. \quad (51)$$

As we mentioned in Sec. III B, the existence of a single negative eigenvalue, of either  $H^+$  or  $H^-$ , suffices to signal the instability. If the Hamiltonian (51) is unbounded from below, or is bounded but has at least one negative eigenvalue, then the RPA instability develops. In 1977, Herbst [17] was able to show that: (a) If  $\alpha > \alpha_c \equiv 4/\pi$ , then the semirelativistic Coulomb Hamiltonian is unbounded from below; (b) If  $\alpha \leq \alpha_c$ , then all eigenvalues are greater than or equal to 0. Specifically, Herbst showed that

$$E \geq 2M\sqrt{1 - \left(\frac{\alpha}{\alpha_c}\right)^2}; \quad \text{for } \alpha \leq \alpha_c. \quad (52)$$

However, for the RPA equations to be stable one must show that all eigenvalues must be positive—a result that does not follow from Eq. (52) at the critical coupling. Although our primary interest in the spectrum of the semirelativistic Coulomb Hamiltonian stems from the stability analysis of Salpeter’s equation, the semirelativistic Coulomb problem is still of considerable theoretical interest [18,19]. Thus, in this subsection we present a variational analysis that, to our knowledge, represents the best estimate of the ground-state energy available in the literature.

To date, no analytic solution for the ground-state energy of the semirelativistic Coulomb problem [Eq. (51)] exists. Thus, we determine an upper bound for the ground-state energy ( $E_0$ ) by using a Rayleigh-Ritz variational method. That is, given a trial wave function  $|\Psi\rangle$ , an upper bound to the ground-state energy is given by the expectation value of  $H$ :

---

<sup>3</sup>In fact, since  $V^-$  is repulsive,  $H^-$  does not even support bound states.

$$E_0 \leq \langle H \rangle \equiv \langle \Psi | H | \Psi \rangle ; \quad \langle \Psi | \Psi \rangle \equiv 1 . \quad (53)$$

In practice, one attempts to include the relevant physics by including a set of variational parameters into  $|\Psi\rangle$ . Then, one minimizes Eq. (53) with respect to those parameters to determine the variational bound and the “optimal”  $|\Psi\rangle$ . In configuration space, the variational wave function is taken to be

$$\Psi(\mathbf{r}) = \sqrt{\frac{1}{4\pi}} R(r) , \quad (54)$$

$$R(r) = N_R \frac{r^\epsilon}{r} e^{-\gamma r} \left[ 1 + c_1(\gamma r) + c_2(\gamma r)^2 + \dots \right] , \quad (55)$$

where the normalization constant is given by

$$N_R = \left[ \frac{(2\gamma)^{1+2\epsilon}}{\sum_{n,m=0}^{\infty} \frac{c_{n-m} c_m}{2^n} \Gamma(1+n+2\epsilon)} \right]^{1/2} . \quad (56)$$

Note that this form of the wave function is appropriate for the  $L = 0$  channel—where the instability should first develop. The expansion for the variational wave function is complete and its form is motivated by the analytic solution of the Dirac-Coulomb problem [20]. In particular, in the weak-coupling limit ( $\alpha \ll 1$ ) one recovers the nonrelativistic result by choosing  $\epsilon = 1$ ,  $\gamma = M\alpha/2$ , and  $c_1 = c_2 = \dots = 0$ , i.e.,

$$E = 2M \left( 1 - \frac{\alpha^2}{8} \right) \quad (57)$$

$$R(r) = \sqrt{\frac{M^3 \alpha^3}{2}} e^{-M\alpha r/2} . \quad (58)$$

In contrast, in the strong-coupling limit ( $\alpha \sim \alpha_c$ ) one expects that the wave function will become localized near the origin, as the energy can benefit from the strong Coulomb attraction. Indeed, the asymptotic behavior of the wave function near the origin is known analytically [21,22]

$$\frac{\tan\left(\frac{\pi}{2}\epsilon\right)}{\left(\frac{\pi}{2}\epsilon\right)} = \frac{\alpha_c}{\alpha} . \quad (59)$$

Note that  $\epsilon \rightarrow 0$  as  $\alpha$  approaches the critical coupling. The variational wave function has also an analytic representation in momentum space. That is,

$$\Psi(\mathbf{k}) = \sqrt{\frac{1}{4\pi}} R(k) , \quad (60)$$

$$R(k) = \frac{1}{k} \sqrt{\frac{2}{\pi}} N_R \sum_{n=0}^{\infty} c_n \gamma^n \frac{\Gamma(1+n+\epsilon)}{(k^2 + \gamma^2)^{(1+n+\epsilon)/2}} \sin \left[ (1+n+\epsilon) \tan^{-1} \left( \frac{k}{\gamma} \right) \right] . \quad (61)$$

One should note that since the constituent quark mass is the only dimensionful parameter in the problem, the dimensionless ratio  $\langle H \rangle / M$  is a function of only the coupling constant  $\alpha$ . In what follows, all expectation values will be written in units of the constituent mass  $M$  and expressed in terms of the dimensionless parameter  $a \equiv \gamma / M$ .

For values of  $\alpha$  not too close to the critical coupling ( $\alpha \lesssim 1.25 < \alpha_c \approx 1.273$ ) the minimization procedure for  $\langle H \rangle / M$  is straightforward and yields the variational energy and optimal parameters ( $a$  and  $\epsilon$ ) that are displayed in Table I. Note, the table reflects the appropriate parameters for the case  $c_1 = c_2 = \dots = 0$ . In contrast, the minimization procedure is highly nontrivial near the critical coupling (and, thus, for  $\epsilon \rightarrow 0$ ) as, both, the kinetic and potential energy diverge as  $1/\epsilon$  (see Appendix). Hence, in order to compute the variational energy for small values of  $\epsilon$  we perform a Laurent expansion of the expectation value of  $H$ , i.e.,

$$\frac{\langle H \rangle}{M} = \frac{h_{-1}}{\epsilon} + h_0 + h_1 \epsilon + \dots \quad . \quad (62)$$

The first term,  $h_{-1}$ , must vanish faster than  $\epsilon \sim (\alpha_c - \alpha)^{1/2}$  as  $\alpha$  approaches the critical coupling; otherwise one would contradict Herbst findings. Indeed, we can extract the critical coupling ( $\alpha_c = 4/\pi$ ) by demanding that the coefficient of the singular term in the series vanishes. Note, we have shown in the appendix that  $h_{-1}$  vanishes as  $(\alpha_c - \alpha)$  in the  $c_1 = c_2 = \dots = 0$  limit (see Eq. A13).

In principle, we could find the variational energy in the  $\alpha = \alpha_c$  limit by minimizing  $h_0$  using the trial wave function (55). In practice, however, we can manage only a small number of variational parameters. Thus, we proceed by, first, minimizing the expectation value of  $H$  using only one term in the polynomial expansion in Eq. (55), i.e., we set  $c_1 = c_2 = \dots = 0$ . Note, most of the details related to this minimization procedure are presented in the appendix. Next, we compute the variational energy by using a two-parameter ( $a$  and  $c_1$ ) wave function. This procedure is straightforward but tedious. However, it enables us to determine the importance of higher-order ‘‘corrections’’ in the polynomial expansion as well as the rate of convergence to the ground-state energy. Our results are summarized below:

$$\frac{\langle H \rangle}{M} = \begin{cases} 0.968583, & \text{for } a = 0.7926 \text{ and } c_1 = 0.0000; \\ 0.968514, & \text{for } a = 0.9359 \text{ and } c_1 = 0.1779. \end{cases} \quad (63)$$

Moreover, an initial study with three variational parameters ( $a$ ,  $c_1$ , and  $c_2$ ) suggests that the two-parameter energy is accurate to, at least, one part per million. To our knowledge this represents the most accurate value for the ground-state energy of the semirelativistic Coulomb problem presented to date. In this way, our small contribution to Herbst work reads: If  $\alpha \leq \alpha_c = 4/\pi$ , then all eigenvalues (in units of  $M$ ) are greater than or equal to 0.968514. Note, our results are consistent with those presented by Raynal and collaborators in a comprehensive study of the semirelativistic Coulomb problem [18]. Their analysis sets lower and upper bounds—differing by less than 1%—for the ground-state energy ( $0.9650 \leq E_0 \leq 0.9686$ ) at  $\alpha = \alpha_c$ .

The remaining question to be answered is how, if at all, does the presence of the linear confining potential alter this stability analysis? The answer is that only the value of the finite piece is changed, at  $\alpha = \alpha_c$ . An explicit calculation gives for the expectation value of the confining potential (with  $c_1 = c_2 = \dots = 0$ )

$$\frac{\langle V \rangle}{M} = \frac{\sigma}{2aM^2} + \frac{\sigma}{aM^2}\epsilon. \quad (64)$$

Thus, there is no  $\mathcal{O}(\epsilon^{-1})$  contribution to the expectation value of  $\langle H \rangle$  coming from the confining potential; only a positive contribution,  $\sigma/2aM^2$ , remains at  $\epsilon \rightarrow 0$ . Note that, because of the additional dimensionful parameter  $\sigma$ , the contribution from the confining potential, unlike the Coulomb contribution, depends on the value of the constituent mass. Hence, for a Coulomb potential of the form of Eq. (44), stability of Salpeter's equation is achieved by demanding that

$$\alpha_s \leq \begin{cases} 4/\pi \approx 1.273, & \text{for timelike;} \\ 1/\pi \approx 0.318, & \text{for vector,} \end{cases} \quad (65)$$

independent of the constituent quark mass.

#### IV. MESON SPECTRA

The heavy quarkonia ( $c\bar{c}$  and  $b\bar{b}$ ) and the light quarkonia ( $u\bar{u}$  and  $s\bar{s}$ ) are investigated in the instantaneous Bethe-Salpeter framework. The analysis is intended to be qualitative in nature, with regard to various effects stemming from the instantaneous approximation; hence a simple generalization of the Cornell potential [23] is employed. The virtue of this approach is its simplicity. The few parameters of the model, constrained by the stability analysis, will emerge from the “best” fit to the meson spectra. One wishes to reproduce the interesting physics (e.g. hyperfine structure) through relativistic effects, rather than by a fine tuning of many parameters.

For the heavy quarkonia, the mass spectra are reasonably described, but details such as the fine and hyperfine structure are less so. For the light quarkonia, the mass spectra are less reasonably described: the pion cannot be accurately modelled within this framework without losing the remaining spectra. At the very least, a more sophisticated phenomenology will be required to accurately describe static properties of the heavy and light quarkonia.

For the remainder of the section, the following program is carried out: the various models to be considered within the Salpeter framework are defined. Then, phenomenological fits to the experimental spectra for heavy mesons are carried out, and a quantitative analysis of the various approximations in the Salpeter framework and their effect on the spectra and splittings is performed. The latter half of the section is concerned with the light mesons.

##### A. Fits to Heavy Mesons

###### 1. Form of the Interaction

The spatial part of the potential is based on the Cornell potential; that is, confinement is parameterized by a linear potential plus a constant, and the asymptotically-free regime is parameterized by an instantaneous OGE potential. Since a good description of the mass spectra of the heavy quarkonia can be obtained with a linear confining potential plus the nonrelativistic reduction of the OGE piece, this is a natural first choice for the Salpeter

equation. (One can, of course, generalize the OGE piece to include running coupling effects motivated from perturbative QCD.)

A mixture of scalar and timelike Lorentz structures for the confining kernel is considered, as a number of authors [24,25] have suggested that an admixture of scalar and timelike confinement is necessary to reproduce the experimental spectra and splittings. The full vector structure is not incorporated in the confining kernel, as this leads to an instability similar to the scalar case. The full vector structure in the Feynman gauge is used for the OGE kernel. Thus, the instantaneous Bethe-Salpeter kernel is parameterized as

$$V(r)\Gamma_{1,2} = [\sigma r + c_\sigma] \left[ x_\sigma \gamma_1^0 \gamma_2^0 + (1 - x_\sigma) \mathbf{1}_1 \mathbf{1}_2 \right] - \left[ \frac{\alpha_s}{r} \right] \gamma_1^\mu \gamma_{2\mu} \quad (66)$$

where  $\sigma$  is the confining string tension,  $x_\sigma$  controls the mixing between scalar and timelike confinement, and  $\alpha_s$  is the (scale-independent) strong coupling constant. One should note that  $\sigma$ ,  $c_\sigma$ ,  $x_\sigma$ ,  $\alpha_s$ , and the quark mass are the only “free” parameters in the approach. From the results of the stability analysis,  $x_\sigma$  and  $\alpha_s$  are restricted to the following values in the Salpeter model in order to have real eigenvalues:

$$0.5 \leq x_\sigma \leq 1.0 \quad ; \quad \alpha_s \leq \frac{1}{\pi} \approx 0.318 \quad .$$

Recall that a typical value for  $\alpha_s$  is 0.24 [26]. One should note that the Breit ( $V^{+-} \equiv 0$ ) model has no such restrictions in principle, saving the possibility of the spectrum becoming unbound from below if the strong coupling becomes too large, similar to the problem encountered for the relativistic Coulomb problem of Section III. However, for comparative purposes,  $x_\sigma$  is restricted to the same range in both models.

## 2. Data and Procedures

One solves for eigenenergies of the Breit (no coupling between positive and negative energy states) and full Salpeter equations, expanding the Salpeter partial-wave amplitudes in an oscillator basis of 20 states per partial wave ( $n_{max}=20$ , or up to 19 nodes in the amplitudes) to insure adequate convergence of the solutions, and with an oscillator parameter value  $\beta=0.6$  GeV suitable for the heavy mesons. Initially, there are six free parameters in the model:  $\sigma$ ,  $\alpha_s$ ,  $M_c$ ,  $M_b$ ,  $x_\sigma$ , and  $c_\sigma$ . The same  $\sigma$ ,  $x_\sigma$ , and  $\alpha_s$  are used to fit both charm and beauty.  $c_\sigma$  is set to zero, assuming the long-range part of the kernel to be less important for the heavy mesons. The scalar-timelike mixing parameter  $x_\sigma$  will be allowed to take only the values 0.5 and 1.0, corresponding to equally-mixed scalar and timelike structure and pure timelike structure, respectively. Hence, the model for the heavy mesons will only have four free parameters, which are determined through minimization of the  $\chi^2$  function

$$\chi^2(\sigma, \alpha_s, M_c, M_b) = \sum_{i=1}^N \frac{(E_{ith} - E_{iexp})^2}{\sigma_{ith}^2 + \sigma_{iexp}^2} \quad (67)$$

using a nonlinear optimization routine [27]. The  $E_{iexp}$  and  $\sigma_{iexp}$  are the experimental masses and associated errors chosen for the fit, here the first two observed  $1^-$  states of b-quarkonium, the first two observed  $0^-$  states and the first five observed  $1^-$  states of charmonium. These

states are used to determine a set of parameters for each choice of Lorentz structure of the confinement. Then, one observes how each of the corresponding spectra agrees with the experimental data overall. The  $E_{ith}$  and  $\sigma_{ith}$  are the calculated masses and their errors within the model (which were taken to be 5-10 MeV). The incorporation of a theoretical error allows one, in principle, to “force” a better fit to some states, at the risk of possibly degrading the fit with respect to the rest of the spectra; however, all states were weighted equally in this regard.

The minimization results for the four parameters for the four models (see Table II for the appropriate definitions) are summarized in Table III, while the charm and beauty quarkonia spectra calculated for each model are summarized in Table IV and Table V. The experimental masses were taken from the Review of Particle Properties [28] (with the exception of the  $h_c$ , which was taken from reference [29]). Graphical depictions of the spectra for each  $J^\pi$  channel are shown for the Breit-Timelike model in Figures 1 and 2.  $J^\pi$  states are named by their main  $^{2S+1}L_J$  components. One notes that for all cases, the parameters fall within commonly accepted ranges for quark potential models.

Figure 3 shows the convergence of the ground and first-excited state energies as the number of states in the basis is increased; adequate convergence is achieved with 20 states in the basis. The numbers quoted for the higher-lying states in Table IV and Table V should be noted with caution, as typically a 10-20 MeV shift in the energies for the fourth-to-fifth eigenstates in going from 18 to 20 basis states is encountered. In particular, the larger differences in the table with respect to the experimental data for the higher excited states are indicative of an insufficient number of states in the basis. Also, all the models appear to be somewhat deficient in comparison to results given by Long [7] and Spence and Vary [26], which examine both Breit and Salpeter equations for a scalar confining kernel and a vector Coulomb kernel. However, those studies allowed more freedom in determining the Salpeter solutions. Long utilizes an oscillator basis but minimizes each eigenstate separately; each state has a different value of  $\beta$  characterizing it, rather than one value for all states. While this procedure does minimize the eigenenergies with fewer states in the basis, the disadvantage is that the eigenstates are not orthogonal, which would be a problem in the calculation of matrix elements, and in ensuring the proper normalization of bound states. Spence and Vary use a spline basis [30] as well as an additional interaction (a so-called “Breit” interaction) which makes comparison more difficult. However, in their work, solutions with imaginary roots (for the light mesons in particular) were discarded on the claim that the imaginary roots appear far from the real roots of interest in the complex plane when the spline basis is chosen as in the study [26]—a procedure that yields (apparently) stable solutions of the Salpeter equation for scalar confinement, in contrast to the results presented here. This latter approach differs drastically from the viewpoint adopted in this work, which is that the onset of imaginary solutions should indicate that a particular interaction is physically inappropriate within the model. (It is rather amusing to note that, when examining a kernel that can lead to instabilities, one can “tune” the oscillator basis to get apparently stable solutions, but that either shifting the value of  $\beta$  or increasing the number of states in the basis (or both) reveals the instability.)

### 3. Comparison of Approximations to Salpeter's Equation

Table VI lists the first four eigenenergies for the pseudoscalar and vector channels, using the Salpeter-Mixed parameters from Table III, to illustrate the various relativistic effects in Salpeter's equation. (These are also illustrated in Figure 4.)

The results show a consistent decrease in the energy of a given level as more relativistic effects are included in the calculation. In going from the Schrödinger case (nonrelativistic kinematics) to the spinless Salpeter case (relativistic kinematics), the energy decreases simply because the nonrelativistic kinetic energy increases quadratically for large momenta, while the relativistic case only increases linearly; since the potential is the same for both cases, the states are more "bound" in the relativistic case. For the Breit case with no lower components, the relativistic normalization ( $\frac{E_k+M}{2E_k}$ ) of the free Dirac spinors suppresses the overall potential for large momenta with respect to the nonrelativistic case, as the normalization varies from 1 in the extreme nonrelativistic limit to  $\frac{1}{2}$  in the extreme relativistic limit. However, both attractive and repulsive contributions to the potential are suppressed, and the energy is still decreased relative to the nonrelativistic case. The inclusion of Z-graphs in the Salpeter case always leads to an added attraction, and consequently to energies reduced relative to the Breit case.

With the introduction of the lower components, the energies are decreased still further, for both the Breit and Salpeter cases. In particular, the spacelike part of the vector potential ( $\gamma_1 \cdot \gamma_2$ ) makes a large contribution. The decrease in going from Breit to Salpeter is realized from the fact that the spacelike part connects the large component of a particle spinor to the large component of an antiparticle spinor in  $V^{+-}$ , hence the contribution from the Z-graphs is much larger than that of the direct graphs alone.

### 4. Fine Structure Analysis

One can obtain information on the spin dependence, and thus on relativistic effects, of the effective potential for the heavy quarkonia by examining the P-wave fine structure. In perturbation theory (which is a good approximation in  $c\bar{c}$  and  $b\bar{b}$ ), to  $\mathcal{O}\left(\frac{1}{M^2}\right)$  one can assess the relative contributions from a Breit reduction of the potential as

$$\mathcal{M}\left({}^{2S+1}P_{J=0,1,2}\right) = \mathcal{M}_0 + \alpha_{SS} \langle \mathbf{S}_1 \cdot \mathbf{S}_2 \rangle + \alpha_{LS} \langle \mathbf{L} \cdot \mathbf{S} \rangle + \alpha_T \langle S_{12} \rangle, \quad (68)$$

where  $\alpha_{SS}$ ,  $\alpha_{LS}$ , and  $\alpha_T$  arise from the spin-spin, spin-orbit, and tensor components of the potential, and

$$\langle \mathbf{S}_1 \cdot \mathbf{S}_2 \rangle = \frac{2S(S+1) - 3}{4} = \begin{cases} +\frac{1}{4}, & \text{for } S=1, \\ -\frac{3}{4}, & \text{for } S=0; \end{cases} \quad (69)$$

$$\langle \mathbf{L} \cdot \mathbf{S} \rangle = \frac{1}{2} [J(J+1) - L(L+1) - S(S+1)] = \begin{cases} -2, & \text{for } {}^3P_0, \\ -1, & \text{for } {}^3P_1, \\ +1, & \text{for } {}^3P_2, \\ +0, & \text{for } {}^1P_1; \end{cases} \quad (70)$$

$$\langle S_{12} \rangle = \langle 12 \left[ (\mathbf{S}_1 \cdot \hat{\mathbf{r}}) (\mathbf{S}_2 \cdot \hat{\mathbf{r}}) - \frac{1}{3} \mathbf{S}_1 \cdot \mathbf{S}_2 \right] \rangle \quad (71)$$



$$= \left\langle \frac{4}{(2L+3)(2L-1)} \left[ \mathbf{S}^2 \mathbf{L}^2 - \frac{3}{2} \mathbf{L} \cdot \mathbf{S} - 3(\mathbf{L} \cdot \mathbf{S})^2 \right] \right\rangle \quad (72)$$

$$= \begin{cases} -4, & \text{for } {}^3P_0, \\ +2, & \text{for } {}^3P_1, \\ -\frac{2}{5}, & \text{for } {}^3P_2, \\ +0, & \text{for } {}^1P_1, \end{cases} \quad (73)$$

(the last two expressions for the tensor component applying for the diagonal elements only), with  $\mathcal{M}_0$  the unperturbed mass. To the extent that perturbation theory is valid for heavy-quark spectroscopy, the couplings describe fundamental parameters of nature. Solving the four equations [Eq. (68)] with the four unknowns yields the data in Tables VII and VIII. Perturbatively, the mass of the  ${}^1P_1$  state should be equal to the center of gravity (COG) of the  ${}^3P_J$  multiplet

$$\text{COG}({}^3P_J) = \frac{1}{9} \left[ 5\mathcal{M}({}^3P_2) + 3\mathcal{M}({}^3P_1) + \mathcal{M}({}^3P_0) \right] \quad , \quad (74)$$

with corrections up to  $\mathcal{O}\left(\frac{1}{M^2}\right)$ . (One notes that  $\mathcal{M}_0$  is equal to the COG in the limit of a zero-range spin-spin interaction). The spin-spin contribution is, except for the Salpeter-Mixed model, an order of magnitude smaller than the tensor and spin-orbit contributions; this can be understood by remembering that the spin-spin term in the Breit reduction is a contact interaction; since the P-wave states have no support at the origin, spin-spin effects are minimized in this channel. (They are not zero here because relativistic corrections in the Breit and Salpeter models regularize the contact term.) The  ${}^1P_1$  state is off in all models, but the error is about 1% at most (0.75% for the Salpeter-Mixed model). For both Breit and Salpeter models, an appropriate mixture of scalar and timelike confinement would be required for a closer match with experiment for the  ${}^1P_1$   $b\bar{b}$  state.

## B. Fits to Light Mesons

### 1. Form of the Interaction

The interaction for the light mesons is taken to be the same form as for the heavy mesons. The flavor-independent OGE kernel, however, leads to degenerate  $\pi$  and  $\eta$  masses; one would need to take higher-order diagrams into account that would lead to a flavor-dependent interaction, such as annihilation diagrams. These, however, are nontrivial to consider in the instantaneous framework and are not treated in this work. It should be noted that there are other QCD-based candidates for flavor-dependent  $q\bar{q}$  interactions that have been computed by t'Hooft and others from instanton effects [31,32]. Such an interaction has been employed in a study similar to this one by Resag *et al.* [33] for an effective description of the light meson spectra.

One change from the heavy quarkonia is that the constant in the confining kernel is permitted as a free parameter. That this is necessary is evinced by Figure 5, which illustrates the  $\pi$ - $\rho$  ground-state splitting, using an up mass  $M_u \equiv M_d = 0.154$  GeV, a string tension  $\sigma = 0.2867$  GeV<sup>2</sup>, and initially a strong coupling  $\alpha_s = 0.2427$ , taken from Spence and Vary [26]. This coupling ( $\alpha_s$ ) is then increased to  $\alpha_s \approx 0.318$ , the maximum allowed value by

the stability analysis in Section III. The maximum  $\pi$ - $\rho$  splitting is less than 400 MeV, still about 230 MeV less than the experimental value. The simplest prescription for adjusting the masses in order to eliminate the difference is to incorporate a constant  $c_\sigma$  into the confining kernel. This “confinement intercept” has been argued for on other grounds: the necessity of regularizing the divergence which appears in treating the linear confining kernel in momentum space leads to the appearance of a negative constant in the potential [34]. It has also been argued that the constant can be understood as arising from the gluon condensate of the nonperturbative vacuum [34]. For heavy systems, its inclusion is not as important, but for light systems (and heavy-light systems) which are affected moreso by the long-range potential, its inclusion is necessary for even a fair description of spin-averaged mass spectra in Schrödinger and relativised Schrödinger (i.e., spinless Salpeter) approaches; hence, its inclusion in the Breit and Salpeter models here is perhaps justified.

Additional complications arise from the fact that in Salpeter’s equation—and in general, any two-body quasi-potential equation—a constant term in the confining kernel does not solely yield an additive shift in the meson mass spectrum but provides a dynamical contribution as well, unlike the Schrödinger or spinless Salpeter cases, where one can view it as a “negative mass” added to the Hamiltonian. Even with other (repulsive) interactions present,  $c_\sigma$  can be increased to the point where the Salpeter solutions exhibit RPA-type instability; the corresponding effect on the Breit solutions is that they become unbounded from below, as with the relativistic Coulomb problem of Section III.

## 2. Data and Procedures

As in the case of heavy quarkonia, eigenenergies of the Breit (no coupling between positive and negative energy states) and full Salpeter equations were solved for, expanding the Salpeter partial-wave amplitudes in an oscillator basis of 20 states per partial wave to insure adequate convergence of the solutions, and with an oscillator parameter value  $\beta=0.3$  GeV suitable for the light mesons. Initially, there are six free parameters in the model:  $\sigma$ ,  $\alpha_s$ ,  $M_u$ ,  $M_s$ ,  $x_\sigma$ , and  $c_\sigma$ , where  $M_s$  is the strange quark mass.  $x_\sigma$  will be allowed to take only the values 0.5 and 1.0, as before.  $\sigma$ ,  $c_\sigma$ ,  $\alpha_s$ , and  $M_u$  are fixed by fitting to the lowest  $1^-$  state, the two lowest  $1^+$  states, and the lowest  $2^+$  state for  $u\bar{u}$ , minimizing the chi-squared function

$$\chi^2(\sigma, c_\sigma, \alpha_s, M_u) = \sum_{i=1}^N \frac{(E_{ith} - E_{iexp})^2}{\sigma_{ith}^2 + \sigma_{iexp}^2} \quad (75)$$

with the errors chosen as for the heavy mesons.  $M_s$  was then obtained by taking the parameters from the fit, and adjusting it to reproduce the  $\phi$  mass.

The minimization results for the four parameters for the four models (Breit-Timelike, Breit-Mixed, Salpeter-Timelike, and Salpeter-Mixed) are summarized in Table IX, while the light and strange quarkonia spectra calculated for each model are summarized in Table X and Table XI; graphical depictions of the spectra for each  $J^\pi$  channel are shown for the Salpeter-Mixed model in Figures 6 and 7.  $J^\pi$  states are named by their main  $^{2S+1}L_J$  components.

The Salpeter-Mixed model is the best model in this case. The problem with it, however, and with the Salpeter-Timelike model, is that in order to fit the  $\rho$ ,  $c_\sigma$  had to be increased

to the point where the  $\pi$  became unstable. The constituent mass values fall within accepted ranges for the Salpeter-Mixed case and the confinement slope is larger than the empirical value  $\sigma \approx 0.2 \text{ GeV}^2$  obtained from spectroscopy. However, it is still in agreement with the lattice result  $\sigma = 0.33_{-0.23}^{+0.82} \text{ GeV}^2$  [34]; although this last comparison is not very significant because of the large error bars. The confinement offset is comparable to that obtained from the prescription  $c_\sigma \approx -2\sqrt{\sigma}$  [34]. The Breit cases fit the  $\rho$ , but cannot reproduce the  $\pi$  at all. That some difficulty should be encountered in describing the pion in these models should not be unexpected. The mass of the  $\pi$  is commonly explained in the framework of broken chiral symmetry, where it corresponds to an almost massless Goldstone boson; such models incorporating chiral symmetry have been investigated by Gross and Milana [35].

In this case, the necessity for the coupling between positive and negative energy states for the light mesons is well illustrated; the Z-graphs provide an additional attraction that may be necessary in describing the  $\pi$  as a deeply bound state of a quark and an antiquark (although in the present model the attraction is too strong in this channel). This need for the  $V^{+-}$  component in the Salpeter equation agrees with the results of Gara *et al.* [24] as well, albeit for different reasons. The  $s\bar{s}$  states are well-described, with the exception of the  $0^+$  states. It is known, however, that these scalar states can not be represented as simple  $q\bar{q}$  states [36]. Note that in this case the strange-quark mass was adjusted to reproduce the  $\phi$ ; the other states are predictions of the model.

## V. CONCLUSIONS

We have used Salpeter's equation to study the light- and heavy-meson spectra. This study was preceded by a stability analysis of Salpeter's equation that proved essential for placing limits on the form of the instantaneous kernel. We stress that because of the RPA structure of Salpeter's equation a stability analysis must always be performed—regardless of the form of the interaction kernel.

The two main results that emerged from the stability analysis are: 1) the Lorentz character of the confining kernel must be timelike or a mixture of scalar and timelike forms, contrary to the usual assumption of pure scalar confinement, and 2) an upper limit of  $\alpha_s = 1/\pi$  was set on the strong coupling constant used in the OGE kernel. This value, and the corresponding value for the ground-state energy, were obtained from a variational solution to the semirelativistic Coulomb problem. To our knowledge this is the best estimate presented to date. Having placed limits on the interaction kernel we proceeded to carry out a detailed study of the heavy and light quarkonia.

Static properties of the heavy and light quarkonia within Salpeter's framework have been examined using a generalization of the Cornell potential. For the heavy quarkonia the relativistic corrections coming into play in the various models were examined. These models included Salpeter and Breit approximations having, either, a timelike or a mixture of scalar and timelike Lorentz structures for the confining potential. Recall that the Breit approximation is obtained by setting  $V^{+-}$  to zero. Meson masses were adequately described in all the models, with the best results obtained using the Breit model with timelike confinement. However, a perturbative study of spin-dependent effects (valid for the heavy quarkonia) reveals that the fine structure (P-wave splittings) and hyperfine structure ( $^3S_1$ - $^3D_1$  splitting) cannot be simultaneously described in any of the models by simply varying the mixing

of scalar and timelike confinement. For the light quarkonia, the mass spectra, except for the pion, are best described by the Salpeter model with mixed scalar-timelike confinement. However, none of the models were able to describe the pion, or equivalently, the  $\pi$ - $\rho$  splitting. For example, in the Breit model the  $\pi$ - $\rho$  splitting is a “mere” 180 MeV. This difference can be pushed up to about 400 MeV in the Salpeter model at the critical coupling; still this value is substantially smaller than the experimental splitting of 630 MeV. The additional attraction needed to describe the pion would appear to rule out using the Breit models for a description of static meson properties. Whether or not this is also sufficient to rule out the use of Salpeter’s equation is not clear at this point. Overall, all of the features of meson spectroscopy could not be simultaneously satisfied using the relatively simple kernel employed here. At the very least, a more sophisticated phenomenology is required, especially for the light mesons and in particular for the pion. It is likely that some form of chirally-invariant model will be needed [35]. It seems clear, however, that keeping the couplings between positive- and negative-energy states is necessary for any realistic description of at least the light spectra, and certainly for a combined heavy-light analysis. Moreover, it should also be clear that regardless of the form of the kernel, the stability analysis used here must be employed in any study that has Salpeter’s equation as the underlying dynamical framework.

## ACKNOWLEDGMENTS

We thank D. Robson for many helpful discussions. This research was supported by the Florida State University Supercomputer Computations Research Institute and the U.S. Department of Energy contracts DE-FC05-85ER250000, DE-FG05-92ER40750, and DE-FG05-86ER40273.

## APPENDIX A: EXTRACTION OF THE COEFFICIENTS TO $\mathcal{O}(\epsilon)$ IN THE VARIATIONAL ENERGY

For a variational wave function of the forms given in Eq. (55) and Eq. (61), one wishes to calculate the matrix elements of the kinetic energy operator and potential operator as  $\epsilon \rightarrow 0$ . These matrix elements diverge logarithmically for large momenta and small radii in their respective integrands; however, one can examine the behavior of the variational energy for small  $\epsilon$ , and determine the critical value of the Coulomb coupling at which the system becomes unbounded. In order to compute the variational energy for small values of  $\epsilon$  we expand  $\langle T \rangle$  and  $\langle V \rangle$  as Laurent series [37] in  $\epsilon$ :

$$\frac{\langle T \rangle}{M} = \frac{t_{-1}}{\epsilon} + t_0 + t_1\epsilon + \dots \tag{A1}$$

$$\frac{\langle V \rangle}{M} = \frac{v_{-1}}{\epsilon} + v_0 + v_1\epsilon + \dots \tag{A2}$$

One wants the leading coefficients  $t_{-1}$ ,  $v_{-1}$  and the zeroth-order ones  $t_0$ ,  $v_0$  as well. By minimizing  $h_0 = t_0 + v_0$  we could find the variational energy in the  $\alpha = \alpha_c$  limit. First we calculate the expectation value of  $H$  using only one term in the polynomial expansion in Eq. (55), i.e., we set  $c_1 = c_2 = \dots = 0$ . Starting with the potential, one has

$$\frac{\langle V \rangle}{M} = -2\alpha \left[ \frac{\gamma\Gamma(2\epsilon)}{M\Gamma(1+2\epsilon)} \right] = -2\alpha \left[ \frac{a\Gamma(2\epsilon)}{(2\epsilon)\Gamma(2\epsilon)} \right] = (-\alpha a) \frac{1}{\epsilon}. \quad (\text{A3})$$

where  $\Gamma(z)$  is the gamma function [37,38]. Note that Eq. (A3) is an exact result; there are no terms of higher order in  $\epsilon$  in the series. The kinetic piece requires a little more care; one first rewrites the integrand using a standard trigonometric identity:

$$\begin{aligned} \frac{\langle T \rangle}{M} &= \int_0^\infty 4\pi k^2 dk \frac{2\sqrt{k^2+M^2}}{M} \frac{1}{4\pi} \left\{ \frac{1}{k} \sqrt{\frac{2}{\pi}} N_R \frac{\Gamma(1+\epsilon)}{(k^2+\gamma^2)^{(1+\epsilon)/2}} \sin \left[ (1+\epsilon) \tan^{-1} \left( \frac{k}{\gamma} \right) \right] \right\}^2 \\ &= \frac{4(2\frac{\gamma}{M})^{1+2\epsilon} [\Gamma(1+\epsilon)]^2}{\pi\Gamma(1+2\epsilon)} \int_0^\infty \frac{dk}{M} \frac{\sqrt{\left(\frac{k}{M}\right)^2+1}}{\left(\frac{k^2+\gamma^2}{M^2}\right)^{1+\epsilon}} \left\{ 1 - \cos^2 \left[ (1+\epsilon) \tan^{-1} \left( \frac{k}{\gamma} \right) \right] \right\}. \quad (\text{A4}) \end{aligned}$$

The second integral in Eq. (A4) is convergent, so there is no ambiguity in setting  $\epsilon = 0$  explicitly. The first integral contains a logarithmic divergence for large  $k$ ; one adds and subtracts this divergence to obtain (with  $a \equiv \gamma/M$  and  $k/M \rightarrow k$ )

$$\frac{\langle T \rangle}{M} = \frac{\langle T \rangle_C}{M} + \frac{\langle T \rangle_D}{M} \quad (\text{A5})$$

$$\frac{\langle T \rangle_C}{M} = \frac{4(2a)^{1+2\epsilon} [\Gamma(1+\epsilon)]^2}{\pi\Gamma(1+2\epsilon)} \int_0^\infty dk \left\{ \frac{\sqrt{k^2+1}-k}{(k^2+a^2)^{1+\epsilon}} - \frac{\sqrt{k^2+1}}{(k^2+a^2)^{1+\epsilon}} \cos^2 \left[ (1+\epsilon) \tan^{-1} \left( \frac{k}{a} \right) \right] \right\} \quad (\text{A6})$$

$$\frac{\langle T \rangle_D}{M} = \frac{4(2a)^{1+2\epsilon} [\Gamma(1+\epsilon)]^2}{\pi\Gamma(1+2\epsilon)} \int_0^\infty dk \frac{k}{(k^2+a^2)^{1+\epsilon}} \quad (\text{A7})$$

$\langle T \rangle_D$  is logarithmically divergent for large momenta, for  $\epsilon = 0$ , so one evaluates the integral for  $\epsilon$  nonzero, then expands about  $\epsilon = 0$  up to  $\mathcal{O}(\epsilon)$ . One then has

$$\frac{\langle T \rangle_D}{M} = \frac{4(2a)^{1+2\epsilon} [\Gamma(1+\epsilon)]^2}{\pi\Gamma(1+2\epsilon)} \frac{1}{2\epsilon a^{2\epsilon}} \quad (\text{A8})$$

$$= \left( \frac{4a}{\pi} \right) \frac{1}{\epsilon} + \frac{8a}{\pi} \ln 2 + \mathcal{O}(\epsilon). \quad (\text{A9})$$

One should note that in going from Eq. (A8) to Eq. (A9), one must be careful to include *all factors* in constructing the series expansion.

The remaining integrals in  $\langle T \rangle_C$  are convergent, and one can set  $\epsilon = 0$  explicitly. Using

$$\cos \left[ \tan^{-1} \left( \frac{k}{a} \right) \right] = \frac{a}{\sqrt{k^2+a^2}}$$

one has

$$\frac{\langle T \rangle_C}{M} = \frac{8a}{\pi} \int_0^\infty dk \left[ \frac{\sqrt{k^2+1}-k}{k^2+a^2} - \frac{\sqrt{k^2+1}a^2}{(k^2+a^2)^2} \right] \quad (\text{A10})$$

$$= \frac{8a}{\pi} \int_0^\infty dk \frac{k^2\sqrt{k^2+1}-k\sqrt{k^2+a^2}}{(k^2+a^2)^2} \quad (\text{A11})$$

$$= \frac{8a}{\pi} \tilde{T}_C(a). \quad (\text{A12})$$

Then, in the limit that  $\epsilon \rightarrow 0$ ,  $\langle H \rangle / M$  can be written as

$$\frac{\langle H \rangle}{M} = \left[ \left( \frac{4}{\pi} - \alpha \right) a \right] \frac{1}{\epsilon} + \frac{8a}{\pi} \ln 2 + \frac{8a}{\pi} \tilde{T}_C(a) + \mathcal{O}(\epsilon), \quad (\text{A13})$$

where  $\tilde{T}_C(a)$  is given in closed form for  $a > 0$  by

$$\tilde{T}_C(a) = \begin{cases} \ln 2 + \ln a - \frac{1}{2} + \frac{1-2a^2}{2a\sqrt{1-a^2}} \tan^{-1} \left( \frac{\sqrt{1-a^2}}{a} \right) & a < 1 \quad ; \\ \ln 2 - 1 & a = 1 \quad ; \\ \ln 2 + \ln a - \frac{1}{2} + \frac{1-2a^2}{2a\sqrt{a^2-1}} \left[ \frac{1}{2} \ln \left( \frac{a+\sqrt{a^2-1}}{a-\sqrt{a^2-1}} \right) \right] & a > 1 \quad . \end{cases} \quad (\text{A14})$$

By demanding that the coefficient of the singular term  $h_{-1}$  in the series vanishes we can extract the critical coupling  $\alpha_c = 4/\pi$ . Furthermore, by minimizing the zeroth-order coefficient  $h_0$  we can derive the variational energy ( $E/M = 0.968583$ ) and the optimal parameter ( $a = 0.7926$ ).

## REFERENCES

- [1] M. A. Shifman, A. I. Vainshtein, and V. I. Zakharov, Nucl. Phys. **B147**, 385 (1979).
- [2] L. J. Reinders, H. Rubinstein, and S. Yazaki, Phys. Rep. **127**, 1 (1985).
- [3] H. Rothe, *Lattice Gauge Theories: An Introduction*, World Scientific Lecture Notes in Physics, Vol. **43**. World Scientific, Singapore, 1992.
- [4] M. Gell-Mann, Phys. Rev. Lett. **8**, 214 (1964).
- [5] S. Godfrey, Nuovo Cimento **102A**, 1 (1989).
- [6] E.E. Salpeter and H.A. Bethe, Phys. Rev. **84**, 1232 (1951).
- [7] C. Long, Phys. Rev. D **30**, 1970 (1984).
- [8] J. Resag and D. Schütte, University of Bonn preprint TK-93-19.
- [9] J. Parramore and J. Piekarewicz, Nucl. Phys. **A585**, 705 (1995).
- [10] J. Piekarewicz, AIP Conference Proceedings No.**269**, 412 (1992); Rev. Mex. Fis. **39**, 542 (1993).
- [11] D.J. Thouless, Nucl. Phys. **21**, 225 (1960); Nucl. Phys. **22**, 78 (1961).
- [12] E.E. Salpeter, Phys. Rev. **87**, 328 (1952).
- [13] N. Ullah and D.J. Rowe, Nucl. Phys. **A163**, 257 (1971).
- [14] B.E. Chi, Nucl. Phys. **A146**, 449 (1970).
- [15] J. Spence and J. Vary, Phys. Rev. D **35**, 2191 (1987).
- [16] K.M. Maung, D.E. Kahuna, and J. W. Norbury, Phys. Rev. D **47**, 1182 (1993).
- [17] Ira W. Herbst, Commun. Math. Phys. **53**, 285 (1977).
- [18] J.C. Raynal, S.M. Roy, V. Singh, A. Martin, and J. Stubbe, Phys. Lett. B **320**, 105 (1994).
- [19] Wolfgang Lucha and Franz F. Schöberl, University of Wien preprint UWThPh-1994-23; hep-ph/9406312.
- [20] J.J. Sakurai, *Advanced Quantum Mechanics*, Addison-Wesley, 1973.
- [21] B. Durand and L. Durand, Phys. Rev. D **28**, 396 (1983).
- [22] J.L. Friar and E.L. Tomusiak, Phys. Rev. C **29**, 1537 (1984).
- [23] E. Eichten, K. Gottfried, T. Kinoshita, K. D. Lane, and T. M. Yan, Phys. Rev. D **17**, 3090 (1978); Phys. Rev. D **21**, 203 (1980).
- [24] Alan Gara, Bernice Durand, Loyal Durand, and L.J. Nickisch, Phys. Rev. D **40**, 843 (1989); Alan Gara, Bernice Durand, and Loyal Durand, Phys. Rev. D **42**, 1651 (1990).
- [25] J.-F. Lagäe, Phys. Rev. D **45**, 317 (1992).
- [26] J. Spence and J. Vary, Phys. Rev. C **47**, 1282 (1993).
- [27] *MINUIT: Function Minimization and Error Analysis, Version 92.1 (March 1992)*, CERN Program Library Long Writeup D506. Application Software Group, Computing and Networks Division, CERN, Geneva, Switzerland.
- [28] K. Hikasa *et al.*, Phys. Rev D **45**, S1 (1992).
- [29] E760 Collaboration, T. A. Armstrong *et al.*, Phys. Lett. **69**, 2337 (1992).
- [30] C. DeBoor, *A Practical Guide to Splines*, Springer, Berlin, 1978.
- [31] G. t'Hooft, Phys. Rev. D **14**, 34432 (1976).
- [32] M. A. Shifman, A. I. Vainshtein, and V. I. Zakharov, Nucl. Phys. **B163**, 46 (1980).
- [33] J. Resag, C.R. Münz, B.C. Metsch, and H.R. Petry, University of Bonn preprint TK-93-13; C.R. Münz, J. Resag, B.C. Metsch, and H.R. Petry, *ibid.*, TK-93-14.
- [34] W. Lucha, F.F. Schöberl, and D. Gromes, Phys. Rep. **200**, 127 (1991).
- [35] F. Gross and J. Milana, Phys. Rev. D **50**, 3332 (1994).

- [36] John Weinstein and Nathan Isgur, *Phys. Rev. D* **41**, 2236 (1990).
- [37] G. Arfken, *Mathematical Methods in Physics*, 3rd ed., 1985.
- [38] I.S. Gradshteyn and I.M. Ryzhik, *Table of Integrals, Series, and Products, corrected and enlarged edition*, Academic Press, New York (1980).



FIGURES

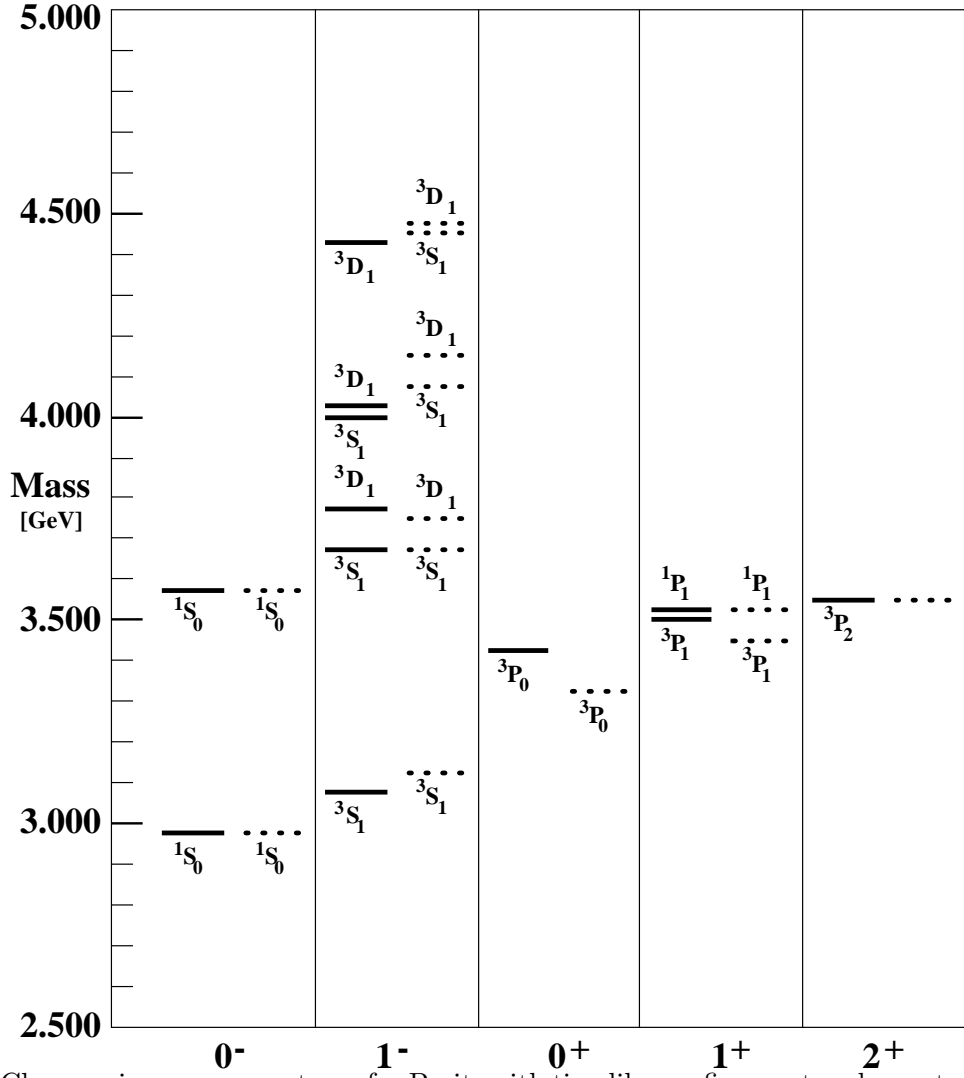


FIG. 1. Charmonium mass spectrum for Breit, with timelike confinement and a vector Coulomb contribution. The experimental numbers are in the left-hand column for each spin-parity. The spectroscopic notation for coupled states is that of the leading component in the calculation.

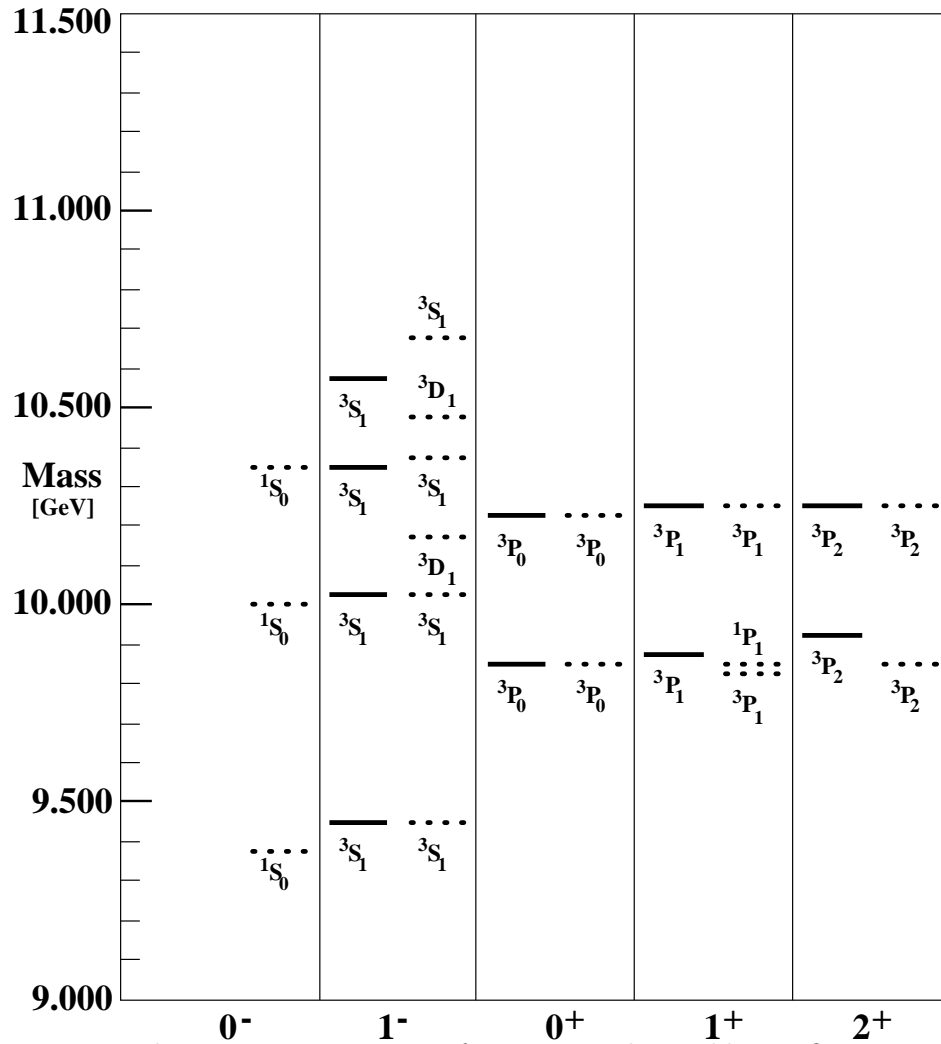


FIG. 2. Beauty quarkonium mass spectrum for Breit, with timelike confinement and a vector Coulomb contribution. The experimental numbers are in the left-hand column for each spin-parity. The spectroscopic notation for coupled states is that of the leading component in the calculation.

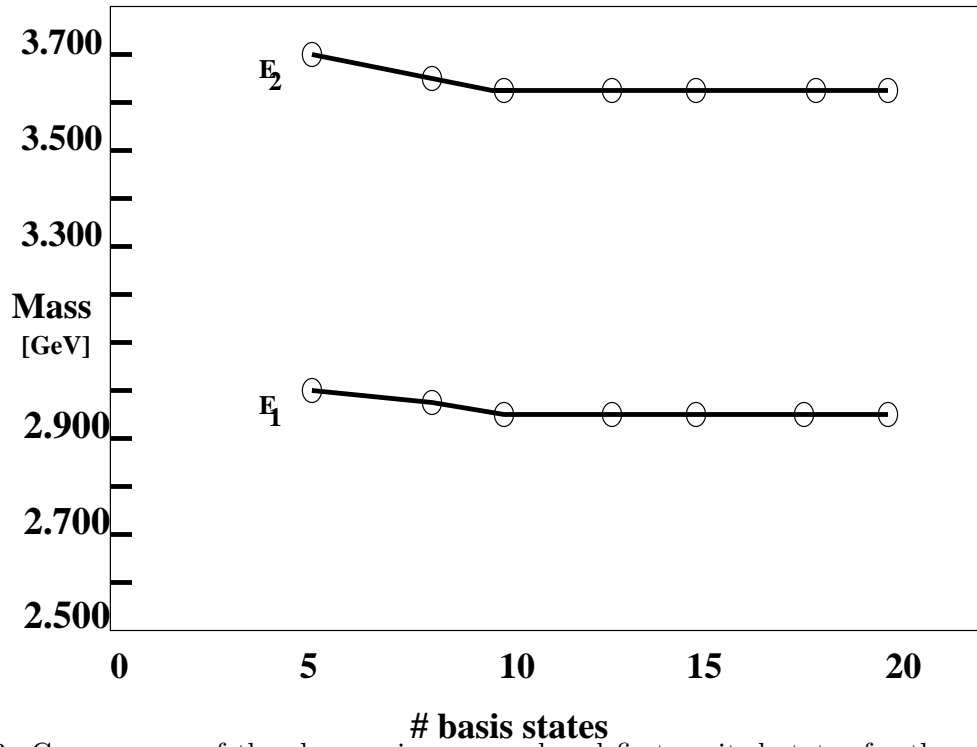


FIG. 3. Convergence of the charmonium ground and first excited states for the pseudoscalar channel as the number of states in the oscillator basis is increased, for Salpeter with mixed confinement as in Table III. The basis parameter is  $\beta=0.6$  GeV for all cases.

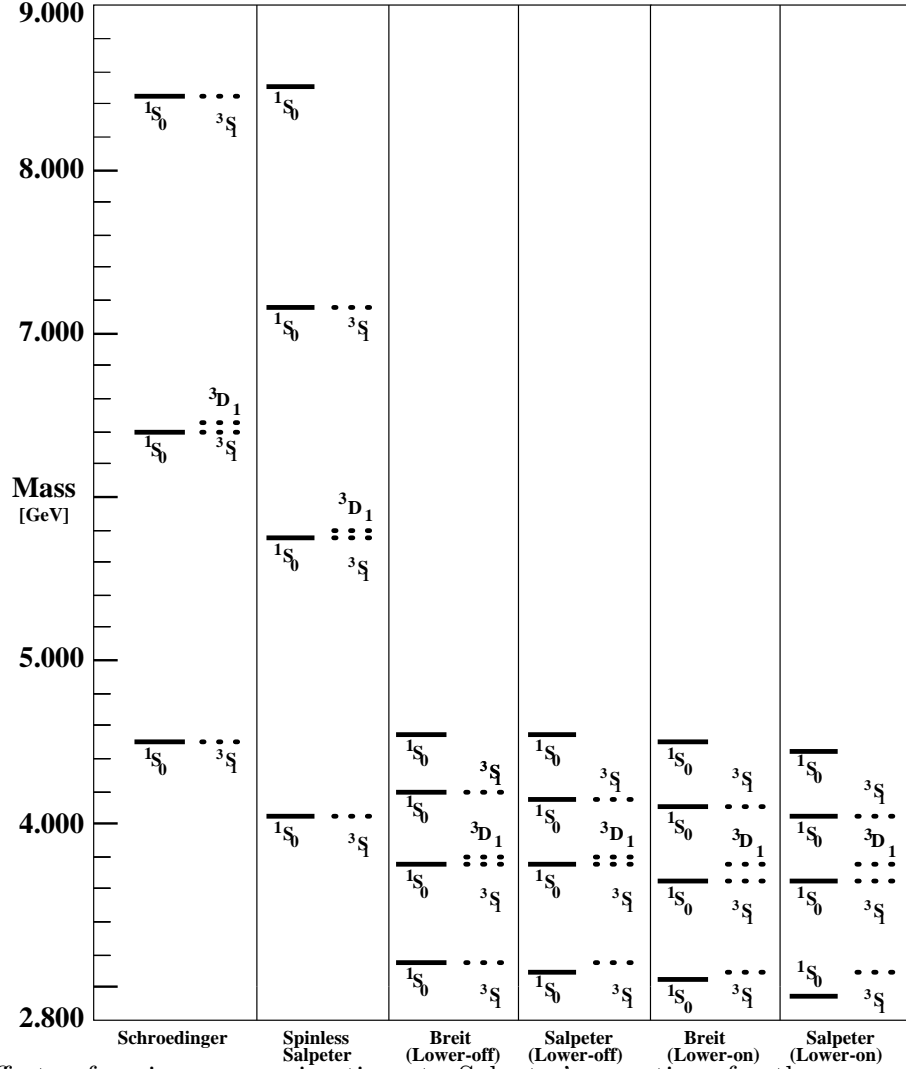


FIG. 4. Effects of various approximations to Salpeter's equation, for the parameters in Table III, for the Salpeter mixed-confinement model, for charmonium.  $0^-$  and  $1^-$  states are in each left-hand and right-hand column, respectively, and the spectroscopic notation quoted is the dominant component of the calculation.

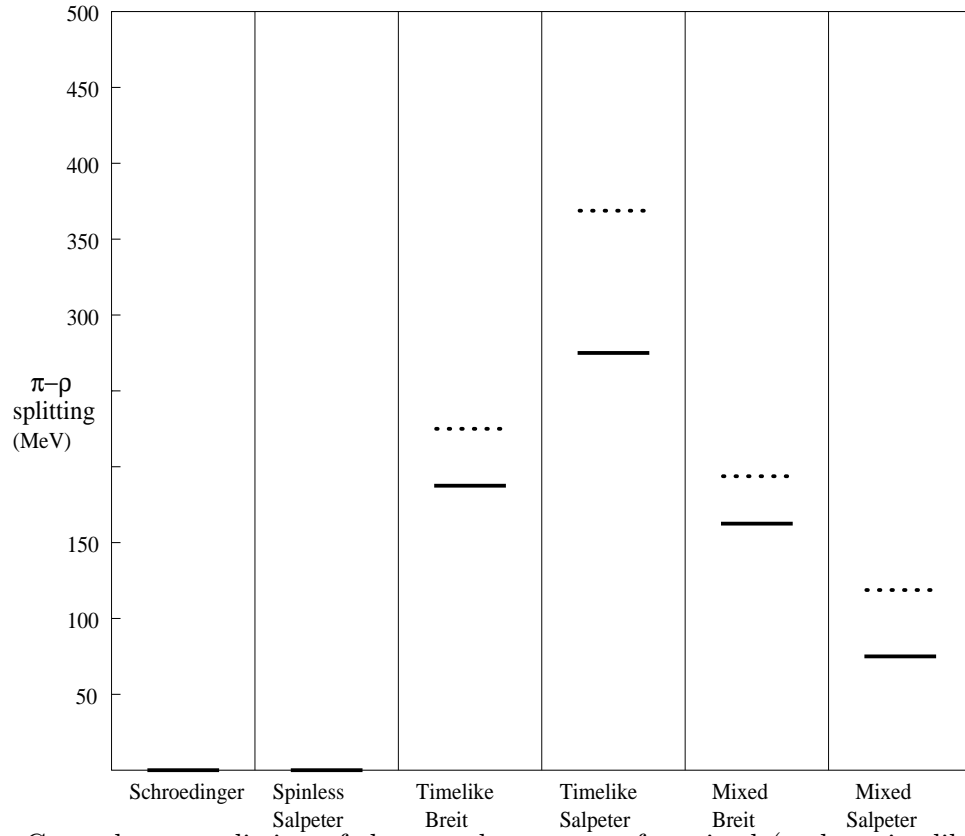


FIG. 5. Ground state splitting of the  $\pi$  and  $\rho$  mesons, for mixed (scalar+timelike) and pure timelike confinement. An oscillator basis with  $n_{max}=20$  and  $\beta=0.3$  GeV was used. The model parameters were taken from reference [26], with the resultant splittings indicated by solid lines. The dotted lines are with  $\alpha_s=0.318$ .

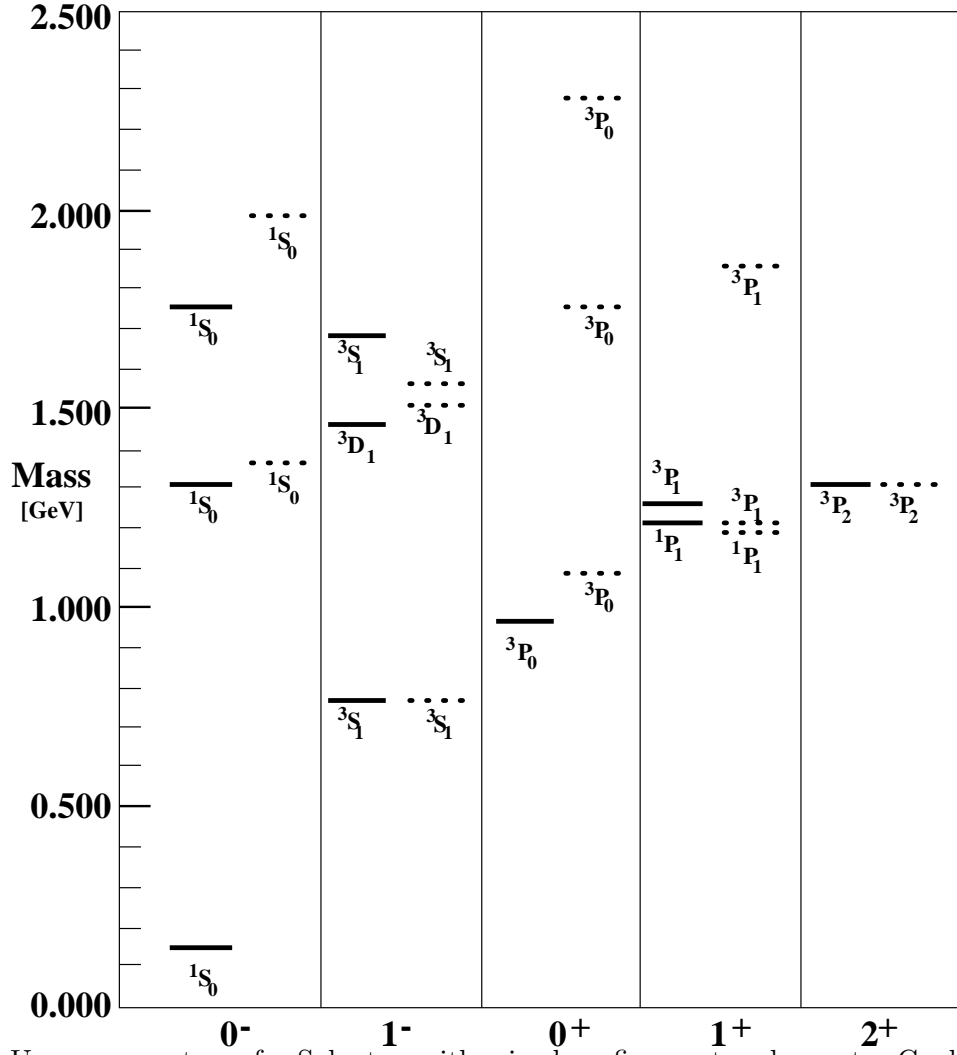


FIG. 6. Up mass spectrum for Salpeter, with mixed confinement and a vector Coulomb contribution. The experimental numbers are in the left-hand column for each spin-parity. The spectroscopic notation for coupled states is that of the leading component in the calculation.

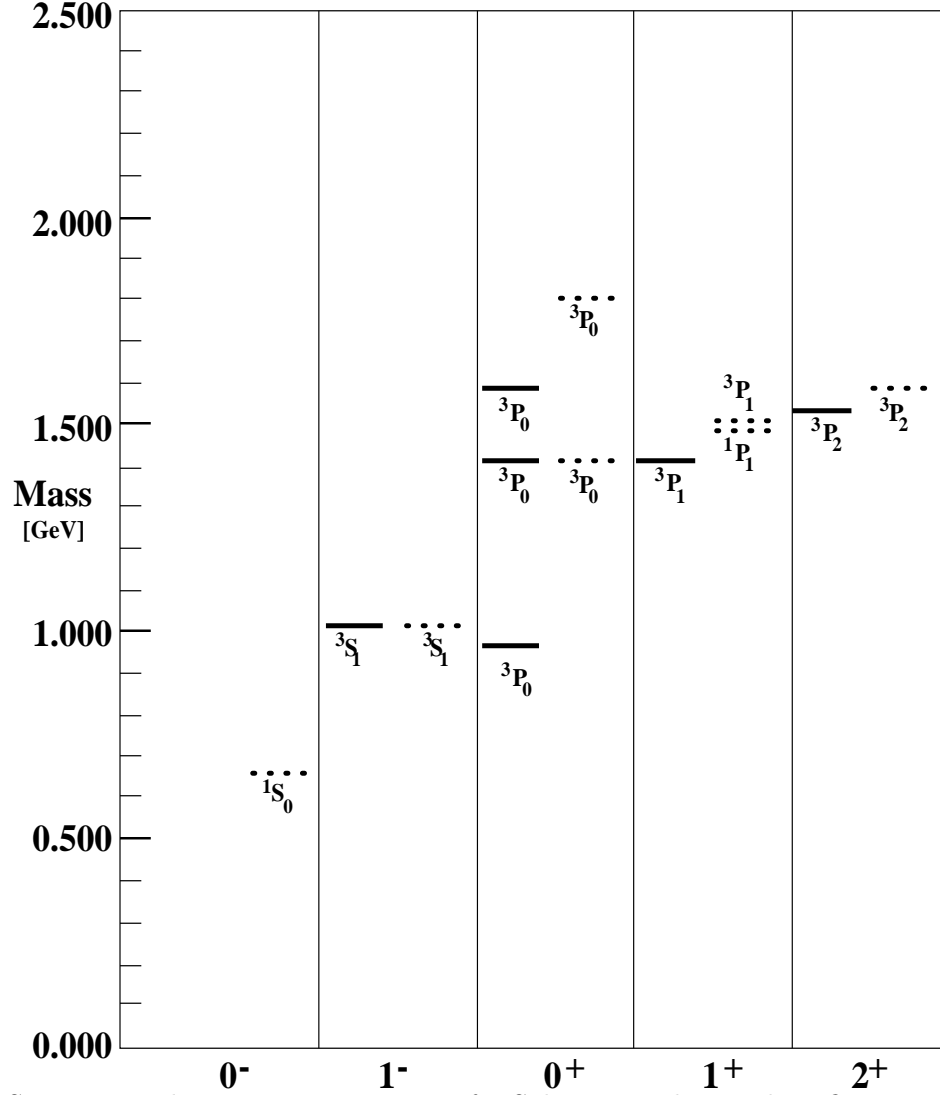


FIG. 7. Strange quarkonium mass spectrum for Salpeter, with mixed confinement and a vector Coulomb contribution. The experimental numbers are in the left-hand column for each spin-parity. The spectroscopic notation for coupled states is that of the leading component in the calculation.

## TABLES

TABLE I. Minimization of the variational energy with respect to the parameters  $\epsilon$  and  $a$  for fixed  $\alpha$ , as  $\alpha$  approaches  $\alpha_c$ .

$\alpha$	$\frac{\langle H \rangle}{M}$	$a$	$\epsilon$
0.100	1.9975	0.0495	0.9861
0.200	1.9899	0.0988	0.9660
0.400	1.9582	0.1956	0.8977
0.600	1.9007	0.2930	0.8041
0.800	1.8081	0.3944	0.6825
1.000	1.6583	0.5071	0.5222
1.200	1.3639	0.6563	0.2703
1.220	1.3106	0.6778	0.2302
1.240	1.2435	0.7033	0.1817
1.260	1.1461	0.7374	0.1144
1.270	1.0581	0.7657	0.05646
1.273	0.9933	0.7854	0.01533
1.2731	0.9874	0.7871	0.01170
1.2732	0.9786	0.7897	0.006226

TABLE II. Definitions of the various models used in the calculations; “Mixed” and “Timelike” refer to the Lorentz structure of the confining kernel. The OGE kernel is always of vector type.

	Mixed	Timelike
Breit	$[V^{+-}=0, x_\sigma=0.5]$	$[V^{+-}=0, x_\sigma=1]$
Salpeter	$[V^{+-}\neq 0, x_\sigma=0.5]$	$[V^{+-}\neq 0, x_\sigma=1]$

TABLE III. Heavy meson parameters for Breit and Salpeter models with mixed (scalar+timelike) and timelike confinement, plus an instantaneous vector OGE contribution. An oscillator basis with  $n_{max}=20$  and  $\beta=0.6$  GeV was employed for the parameter optimization.

Parameters	Breit Mixed	Breit Timelike	Salpeter Mixed	Salpeter Timelike
$M_c$ [GeV]	1.168	1.379	1.251	1.126
$M_b$ [GeV]	4.573	4.781	4.623	4.561
$\sigma$ [GeV <sup>2</sup> ]	0.2991	0.1937	0.2570	0.2743
$\alpha_s$	0.2678	0.4875	0.2872	0.2165



TABLE IV. Charm quarkonia masses in GeV for Breit and Salpeter models with mixed (scalar+timelike) and timelike confinement, plus an instantaneous vector OGE contribution, for the parameters as in Table III. The calculated states are aligned with the observed states according to their spin parity, starting from the lowest mass values. An asterisk on an observed value indicates a state employed in the fits. An oscillator basis with  $n_{max}=20$  and  $\beta=0.6$  GeV was employed for all states.

Meson	$J^\pi$	$^{2S+1}L_J$	$M_{expt}$	Breit Mixed	Breit Timelike	Salpeter Mixed	Salpeter Timelike
$\eta_c$	$0^-$	$^1S_0$	2.979*	2.984	2.977	2.958	2.968
$J/\psi$	$1^-$	$^3S_1$	3.097*	3.044	3.111	3.099	3.056
$\chi_{c0}$	$0^+$	$^3P_0$	3.415	3.360	3.326	3.372	3.338
$\chi_{c1}$	$1^+$	$^3P_1$	3.511	3.421	3.468	3.412	3.424
$h_c$	$1^+$	$^1P_1$	(3.526)	3.440	3.514	3.468	3.455
$\chi_{c2}$	$2^+$	$^3P_2$	3.556	3.467	3.562	3.499	3.513
$\eta_c$	$0^-$	$^1S_0$	(3.594)*	3.645	3.597	3.622	3.647
$\psi$	$1^-$	$^3S_1$	3.685*	3.688	3.675	3.693	3.705
$\psi$	$1^-$	$^3D_1$	3.770*	3.726	3.755	3.739	3.732
$\psi$	$1^-$	$^3S_1$	4.040*	4.167	4.099	4.134	4.218
$\psi$	$1^-$	$^3D_1$	4.159*	4.192	4.152	4.162	4.234
$\psi$	$1^-$	$^3S_1$		4.566	4.459	4.499	4.659
$\psi$	$1^-$	$^3D_1$	4.415	4.583	4.499	4.519	4.669

TABLE V. Beauty quarkonia masses in GeV for Breit and Salpeter models with mixed (scalar+timelike) and timelike confinement, plus a vector OGE (instantaneous Coulomb) contribution, for the parameters as in Table III. The calculated states are aligned with the observed states according to their spin parity, starting from the lowest mass values. An asterisk on an observed value indicates a state employed in the fits. An oscillator basis with  $n_{max}=20$  and  $\beta=0.6$  GeV was employed for all states.

Meson	$J^\pi$	$^{2S+1}L_J$	$M_{expt}$	Breit Mixed	Breit Timelike	Salpeter Mixed	Salpeter Timelike
$\eta_b$	$0^-$	$^1S_0$		9.440	9.377	9.373	9.432
$\Upsilon$	$1^-$	$^3S_1$	9.460*	9.468	9.459	9.485	9.488
$\chi_{b0}$	$0^+$	$^3P_0$	9.860	9.821	9.853	9.825	9.807
$\chi_{b1}$	$1^+$	$^3P_1$	9.892	9.843	9.905	9.850	9.827
$\chi_{b1}$	$1^+$	$^1P_1$		9.850	9.921	9.841	9.826
$\chi_{b2}$	$2^+$	$^3P_2$	9.913	9.858	9.940	9.865	9.845
$\eta_b$	$0^-$	$^1S_0$		9.995	9.992	9.949	9.962
$\Upsilon$	$1^-$	$^3S_1$	10.023*	10.013	10.023	9.999	9.994
$\Upsilon$	$1^-$	$^3D_1$		10.112	10.164	10.100	10.077
$\chi_{b0}$	$0^+$	$^3P_0$	10.232	10.245	10.230	10.214	10.211
$\chi_{b1}$	$1^+$	$^3P_1$	10.255	10.263	10.266	10.236	10.229
$\chi_{b2}$	$2^+$	$^3P_2$	10.268	10.277	10.293	10.249	10.244
$\eta_b$	$0^-$	$^1S_0$		10.397	10.350	10.332	10.352
$\Upsilon$	$1^-$	$^3S_1$	10.355	10.412	10.371	10.367	10.375
$\Upsilon$	$1^-$	$^3D_1$		10.477	10.462	10.434	10.432
$\Upsilon$	$1^-$	$^3S_1$	10.580	10.748	10.655	10.675	10.702

TABLE VI. Various relativistic effects in Salpeter's equation displayed in the pseudoscalar and vector channels for charmonium, using the parameters from the Salpeter-mixed model as in Table III.  $S$  and  $D$  label the dominant  $L$ -wave component in the calculated energy. *Lower on* and *Lower off* refer to the lower components of Dirac spinors being present or not, respectively, in the calculation.

$J^\pi$	Schrödinger	Spinless Salpeter	Breit Lower-off	Salpeter Lower-off	Breit Lower-on	Salpeter Lower-on
$0^-$	4.302 (S)	4.140 (S)	3.154 (S)	3.104 (S)	3.049 (S)	2.958 (S)
	6.407 (S)	5.774 (S)	3.761 (S)	3.740 (S)	3.659 (S)	3.623 (S)
	8.464 (S)	7.193 (S)	4.200 (S)	4.187 (S)	4.108 (S)	4.084 (S)
	10.499 (S)	8.480 (S)	4.562 (S)	4.552 (S)	4.481 (S)	4.461 (S)
$1^-$	4.302 (S)	4.140 (S)	3.154 (S)	3.149 (S)	3.107 (S)	3.099 (S)
	6.407 (S)	5.774 (S)	3.761 (S)	3.758 (S)	3.699 (S)	3.693 (S)
	6.442 (D)	5.880 (D)	3.817 (D)	3.816 (D)	3.747 (D)	3.739 (D)
	8.464 (S)	7.193 (S)	4.200 (S)	4.198 (S)	4.141 (S)	4.134 (S)

TABLE VII. Spin-dependent parameters for spin-spin, spin-orbit, and tensor contributions to the effective potential for charmonium. “COG” refers to the center of gravity of a given multiplet. All values listed are in units of [GeV].

Parameter	Experiment	Breit Mixed	Breit Timelike	Salpeter Mixed	Salpeter Timelike
COG( ${}^3P_J$ )	3.525	3.440	3.504	3.456	3.464
${}^1P_1$	3.526	3.440	3.514	3.468	3.455
$\mathcal{M}_0$	3.526	3.440	3.507	3.459	3.462
$\alpha_{SS}$	-0.001	-0.0002	-0.010	-0.012	0.009
$\alpha_{LS}$	0.035	0.029	0.063	0.043	0.051
$\alpha_T$	0.010	0.005	0.013	-0.001	0.006

TABLE VIII. Spin-dependent parameters for spin-spin, spin-orbit, and tensor contributions to the effective potential for beauty quarkonium. “COG” refers to the center of gravity of a given multiplet. The given  ${}^1P_1$  experimental mass is actually the calculated COG. All values listed are in units of [GeV].

Parameter	Experiment	Breit Mixed	Breit Timelike	Salpeter Mixed	Salpeter Timelike
COG( ${}^3P_J$ )	9.900	9.849	9.919	9.852	9.833
${}^1P_1$	9.900	9.850	9.921	9.841	9.826
$\mathcal{M}_0$	9.900	9.849	9.919	9.852	9.833
$\alpha_{SS}$	0.0001	-0.001	-0.002	0.015	0.009
$\alpha_{LS}$	0.014	0.010	0.023	0.010	0.011
$\alpha_T$	0.003	0.002	0.005	0.002	0.002

TABLE IX. Light meson parameters for Breit and Salpeter models with mixed (scalar+timelike) and timelike confinement, plus an instantaneous OGE contribution. An oscillator basis with  $n_{max}=20$  and  $\beta=0.3$  GeV was employed for the data fitting.

Parameter	Breit Mixed	Breit Timelike	Salpeter Mixed	Salpeter Timelike
$M_u$ [GeV]	0.2862	0.3393	0.3229	0.4196
$M_s$ [GeV]	0.5500	0.5720	0.5610	0.6240
$\sigma$ [GeV] <sup>2</sup>	0.3841	0.2576	0.3744	0.2574
$c_\sigma$ [GeV]	-1.448	-1.089	-1.427	-1.157
$\alpha_s$	0.2919	0.3064	0.2690	0.2690

TABLE X. Light quarkonia masses in GeV for Breit and Salpeter models for the parameters as in Table IX. The calculated states are aligned with the observed states according to their spin parity. An asterisk on an observed value indicates a state employed in fitting. An “I” indicates imaginary eigenvalues.

Meson	$J^\pi$	$^{2S+1}L_J$	$M_{expt}$	Breit Mixed	Breit Timelike	Salpeter Mixed	Salpeter Timelike
$\pi$	$0^-$	$^1S_0$	0.140	0.627	0.642	I	I
$\rho$	$1^-$	$^3S_1$	0.768*	0.771	0.770	0.768	0.769
$a_0$	$0^+$	$^3P_0$	0.983	1.066	0.839	1.014	0.787
$b_1$	$1^+$	$^1P_1$	1.232*	1.203	1.153	1.195	1.148
$a_1$	$1^+$	$^3P_1$	1.260*	1.169	1.033	1.205	1.081
$\pi'$	$0^-$	$^1S_0$	1.300	1.447	1.368	1.370	1.332
$a_2$	$2^+$	$^3P_2$	1.318*	1.320	1.320	1.319	1.317
$\rho'$	$1^-$	$^3D_1$	1.47	1.482	1.316	1.512	1.360
?	$2^-$	$^3D_2$		1.597	1.504	1.622	1.532
$\pi_2$	$2^-$	$^1D_2$	1.670	1.607	1.566	1.627	1.573
$\rho''$	$1^-$	$^3S_1$	1.70	1.556	1.451	1.570	1.460
$\pi''$	$0^-$	$^1S_0$	1.77	2.042	1.940	2.006	1.928

TABLE XI. Strange quarkonia masses in GeV for Breit and Salpeter models for the parameters as in Table IX. The calculated states are aligned with the observed states according to their spin parity. An asterisk on an observed value indicates a state employed in fitting.

Meson	$J^\pi$	$^{2S+1}L_J$	$M_{expt}$	Breit Mixed	Breit Timelike	Salpeter Mixed	Salpeter Timelike
?	$0^-$	$^1S_0$		0.928	0.929	0.640	0.741
$f_0$	$0^+$	$^3P_0$	0.974	1.401	1.198	1.422	1.164
$\phi$	$1^-$	$^3S_1$	1.019*	1.019	1.020	1.019	1.020
$f_0$	$0^+$	$^3P_0$	1.400	1.764	1.570	1.784	1.859
$f_1$	$1^+$	$^3P_1$	1.426	1.487	1.346	1.501	1.369
$f_1$	$1^+$	$^1P_1$		1.515	1.431	1.483	1.412
$f_2'$	$2^+$	$^3P_2$	1.525	1.577	1.587	1.581	1.536
$f_0$	$0^+$	$^3P_0$	1.587	2.647	2.398	2.636	2.390
?	$2^-$	$^3D_2$		1.920	1.777	1.927	1.788
?	$2^-$	$^1D_2$		1.928	1.822	1.923	1.817